Puzzling Connections between Behavior, Spectral Photoreceptor Classes and Visual System Simplification: Branchiopod Crustaceans and Unconventional Color Vision

by

Nicolas Lessios

A Dissertation Presented in Partial Fulfillment
of the Requirements for the Degree
Doctor of Philosophy

Approved June 2016 by the
Graduate Supervisory Committee:

Ronald Rutowski, Co-Chair
Jonathan Cohen, Co-Chair
John Harrison
Susanne Neuer
Kevin McGraw

ARIZONA STATE UNIVERSITY

August 2016

ABSTRACT

Why do many animals possess multiple classes of photoreceptors that vary in the wavelengths of light to which they are sensitive? Multiple spectral photoreceptor classes are a requirement for true color vision. However, animals may have unconventional vision, in which multiple spectral channels broaden the range of wavelengths that can be detected, or in which they use only a subset of receptors for specific behaviors. Branchiopod crustaceans are of interest for the study of unconventional color vision because they express multiple visual pigments in their compound eyes, have a simple repertoire of visually guided behavior, inhabit unique and highly variable light environments, and possess secondary neural simplifications. I first tested the behavioral responses of two representative species of branchiopods from separate orders, *Streptocephalus mackini* Anostracans (fairy shrimp), and *Triops longicaudatus* Notostracans (tadpole shrimp). I found that they maintain vertical position in the water column over a broad range of intensities and wavelengths, and respond behaviorally even at intensities below those of starlight. Accordingly, light intensities of their habitats at shallow depths tend to be dimmer than terrestrial habitats under starlight. Using models of how their compound eyes and the first neuropil of their optic lobe process visual cues, I infer that both orders of branchiopods use spatial summation from multiple compound eye ommatidia to respond at low intensities. Then, to understand if branchiopods use unconventional vision to guide these behaviors, I took electroretinographic recordings (ERGs) from their compound eyes and used models of spectral absorptance for a multimodel selection approach to make inferences about the number of photoreceptor classes in their eyes. I infer that both species have four spectral classes of photoreceptors

that contribute to their ERGs, suggesting unconventional vision guides the described behavior. I extended the same modeling approach to other organisms, finding that the model inferences align with the empirically determined number of photoreceptor classes for this diverse set of organisms. This dissertation expands the conceptual framework of color vision research, indicating unconventional vision is more widespread than previously considered, and explains why some organisms have more spectral classes than would be expected from their behavioral repertoire.

ACKNOWLEDGMENTS

I thank my advisor Ron Rutowski for his unfailing optimism, his support of an unconventional research topic, and his role in teaching me to be a mentor. I thank my committee: Susanne Neuer, Jon Harrison, and Kevin McGraw for their support and feedback throughout my degree, and especially Jon Cohen for his continued discussions over the years as well as hosting me during two research visits. I also thank Julie Mustard for her input early in graduate school. I thank former graduate members of the Rutowski lab, Kim Pegram and Brett Seymoure, for sharing an office, lively discussions and their food with me. I thank the undergraduates of the Rutowski lab and look forward to finding out the places they have gone over the next few years. I thank former graduate students at SoLS: Matt Toomey, Mike Butler, Lisa Taylor, Rusty Ligon, Josh Gibson, and others who made graduate school a welcoming environment. I also thank current graduate students Jason Borchert, Chris Jernigan, Ti Eriksson, Owen McKenna, Meghan Duell, Rick Simpson and others who continue to make SoLS a welcoming environment.

Finally I owe a lot to my parents, Haris Lessios and Kristin Neva, and last but not least, Julia Damerow for her love and understanding

TABLE CONTENTS

CHAPTER Page

LIST OF TABLES

Table Page

LIST OF FIGURES

Figure Page

PREFACE

Visual ecologists seek to answer how organisms and their visual systems are adapted and how they are constrained in using environmental information (Stevens, 2013). All animal visual systems transduce light into neural signals using absorptive molecular complexes called visual pigments (Bowmaker, 1999). The cells that contain visual pigments and are responsible for producing neural signals are photoreceptor cells (Cronin, Johnsen, Marshall, & Warrant, 2014a). Many animals have multiple classes of photoreceptors that vary in the spectral sensitivity of their visual pigments. A main goal of visual ecology is to answer the following question: why do animals express multiple spectral classes of photoreceptors?

Two alternative hypotheses potentially address this question: 1) Multiple spectral photoreceptor classes are required for color vision, the ability to perform spectral discrimination and 2) Multiple spectral photoreceptor classes broaden the range of wavelengths that can be detected by a visual system pathway. In this dissertation, I use branchiopod crustaceans to test these hypotheses. Branchiopods are of interest because they express multiple visual pigments in their compound eyes (Kashiyama, Seki, Numata, & Goto, 2009), they have a simple repertoire of visually guided behavior, they inhabit unique and highly variable light environments, and they possess secondary simplifications to the neuropils of their optic lobe that are unique among arthropods.

Vision research has been effective in testing the Sensory Drive hypothesis (Endler, 1992) which addresses the question of the adaptive significance of visual system tuning due to the coevolution of visual signalers and receivers. This has led to work with clear hypotheses and predictions, which have been tested very successfully within species

(Morehouse & Rutowski, 2010), (Toomey & McGraw, 2009) and within small groups of related species (Seehausen et al., 2008). This work has supported predicted patterns in physiological mechanisms of vision, indicating that there is often an adaptive match between stimuli which are relevant to fitness and absorption maxima of the visual system (Cronin & Forward, 1988; Forward, Cronin, & Douglass, 1988).

Though it also falls within the Sensory Drive Hypothesis, few researchers have been able to isolate and test adaptive hypotheses of ecological selection on the behavior and vision of organisms from the perspective of comparing physical limits on reception using naturally coexisting taxa (Cummings, 2007). One reason for the lack of studies comparing these limits is that identifying ecologically relevant information becomes more challenging for taxa that have multiple visual pigments such as birds (Osorio & Vorobyev, 2005), cichlid fish (Carleton, Spady, & Kocher, 2006), or in the most extreme examples, mantis shrimp (Cronin, 2005)

Luminance, unconventional, and true color vision: multiple visual pigments do not always indicate true color vision

Visual pigments are light-sensitive molecular complexes that are found in all animal visual systems (Land & Nilsson, 2012). They consist of an opsin protein bound to a chromophore (vitamin A derivative). The chromophore itself is maximally sensitive to ultraviolet light, but it is the interaction between the opsin and the chromophore that subsequently determine the wavelength sensitivity of a visual pigment. Chromophores change conformation when they absorb photons, forcing the opsin to also change conformation, initiating the signal transduction pathway that leads to the generation of

electrical signals in response to light. Visual pigments are characterized by their wavelength of maximal absorption, λ_{max}. At the cellular level, visual pigment molecules are stacked into layers along the exterior of each photoreceptor cell. (Bradbury & Vehrencamp, 1998).

There are several requirements that the visual system must meet for an animal to be able to use color vision to obtain spectral information from light. The first requirement is for the visual system to have two or more spectral classes of visual pigments that are housed in separate photoreceptor cells. The second requirement underlying true color vision is that the neural signals of these photoreceptors must then be compared synaptically at a further processing stage in the visual system. Because the underlying mechanism is a comparison between photoreceptor outputs, the resulting signal is largely independent of intensity. This is referred to as an opponent interaction and is the basis for true color vision (Menzel, 1979).

However, in some animals there is evidence that the neural signals from photoreceptor cells that have separate classes of visual pigments are not compared exclusively in opponent interactions. Instead, they can be summed, effectively reducing or eliminating the number of potential opponent interactions, or an organism can use only a subset of the spectral classes they possess, mapped to specific behaviors. Such cases have been identified as "unconventional color vision" has been applied (Marshall & Arikawa, 2014). However, these behaviors also include those which are guided by luminance vision. Therefore, I will refer to this type of vision as "unconventional vision", rather than unconventional "color" vision, from here onwards in this dissertation.

The hierarchy of these definitions and the rationale for using the term "unconventional vision" is summarized in Figure i.1**.** A clear example of unconventional vision is that in dim light honeybees sum the outputs of three spectral types of their photoreceptors to return to the hive (Menzel & Greggers, 1985). Another would be how talitrid amphipods use a single spectral photoreceptor class which is maximally sensitive to middle wavelengths to return to their burrows above the high tide line after foraging behavior, but use a separate, short wavelength sensitive photoreceptor class for sun compass navigation. (Cohen, Cronin, Lessios, & Forward, 2010; Forward, Bourla, Lessios, & Cohen, 2009).

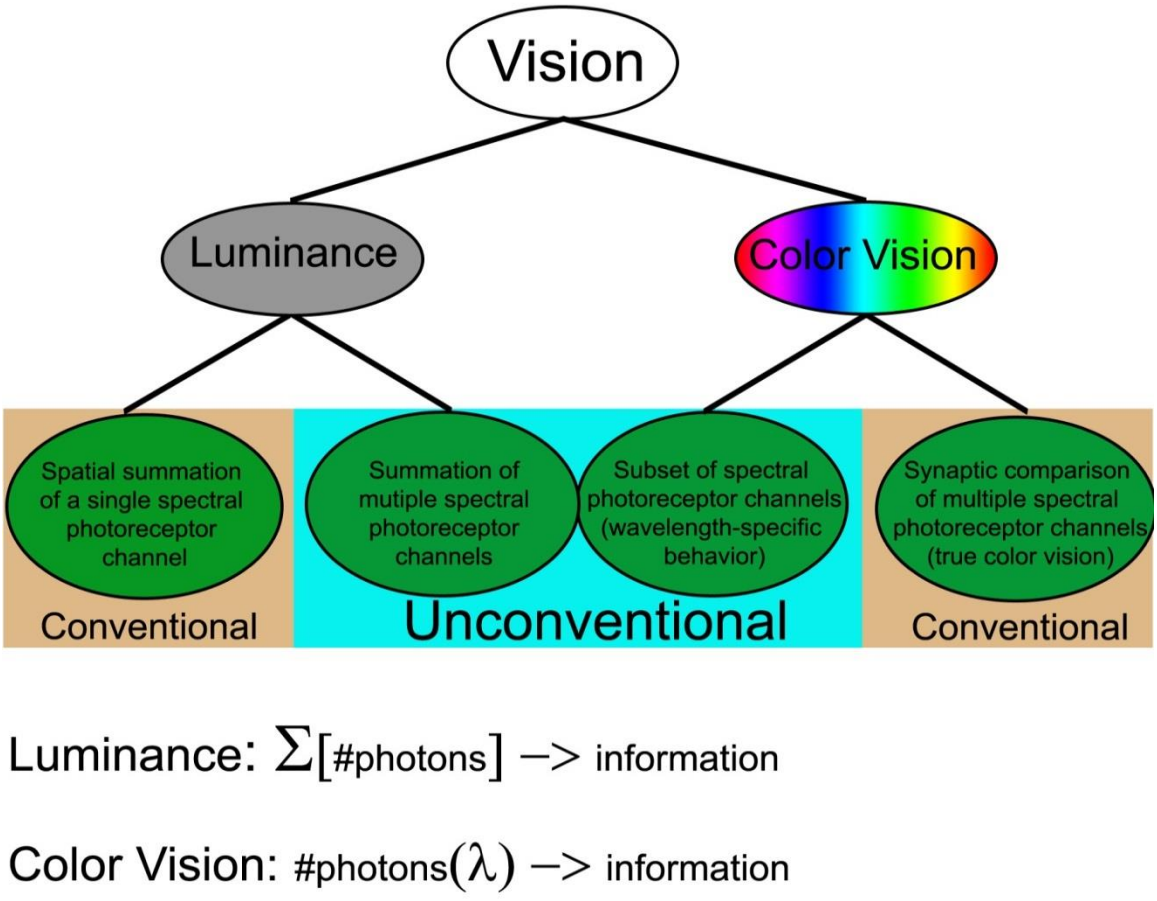

Figure i.1. Conceptual Map of Unconventional Vision. This figure highlights the main conclusions of this dissertation regarding what constitutes "unconventional vision".

As represented in Figure i.1, there are inherent trade-offs in information capture between luminance from a single spectral class, and true color vision. Due to spatial and temporal summation, luminance visual pathways can be more sensitive, and are often involved with motion detection. However, true color vision is more reliable in environments where intensity is variable because channels are compared, rather than summed (Kelber, 2005). This distinction is exemplified in human photoreceptor types. Rod photoreceptors possess only a single visual pigment type, and their outputs are summed for efficient luminance vision in dim light. Cone photoreceptors possess three visual pigment types, and opponent comparisons are made between combinations of cone photoreceptor types (Bradbury & Vehrencamp, 1998). The trade-off in this case would be that rod photoreceptors are pooled to overcome a minimum intensity to provide a reliable signal to noise ratio, whereas cone photoreceptors can be used for spectral discrimination under more variable intensity conditions.

In reality, the association between dim light environments and luminance vision is not rigid. Several animals (nocturnal hawkmoths, geckos) employ color vision even in very dim light intensities, such as those of starlight (Kelber, Balkenius, & Warrant, 2002; Kelber & Lind, 2010), but this comes at a cost for spatial and temporal resolution. A given organism will experience a range of intensities and will often have multiple visual modalities used for separate behaviors if it has general purpose eyes (Land & Nilsson, 2005). Nevertheless, if the natural range of variation of the light environment is understood as a relevant selective pressure, it is possible to make predictions if a true color vision system can be employed (Kelber, 2005).

Color processing in Arthropoda and Pancrustacea

Both true color and luminance visual pathways are found in all insect taxa examined so far (Pichaud, Briscoe, & Desplan, 1999). In most Pancrustaceans, a clade of arthropods which mainly consists of insects and crustaceans, the photoreceptor cells which are found in their compound eyes are segregated into color and luminance pathways. Furthermore, just as for humans, these separate pathways have parallel circuitry that is integrated only in neural structures downstream (Kelber & Henze, 2013). In each ommatidium of the compound eyes of *Drosophila*, the best known Pancrustacean visual system, six photoreceptor cells (numbered R1-R6) all express a single spectral class of visual pigment, and contribute to a luminance pathway in which the photoreceptor axons terminate in the first neuropil of the optic lobe (lamina, see Figure i.2 below), whereas the rest (R7-R8) terminate in the second neuropil of the optic lobe (medulla), passing through the lamina with little or no summation. The point of these photoreceptor comparisons is that in order for synaptic comparisons to be made for true color vision, information from spectral photoreceptor classes must first be anatomically separated.

In Pancrustaceans, the synaptic connections used for color comparisons are found mainly in the medulla of the optic lobe (Dyer, Paulk, & Reser, 2011; Kleinlogel, Marshall, Horwood, & Land, 2003; Melnattur et al., 2014; Morante & Desplan, 2008; Paulk, Dacks, & Gronenberg, 2009; Strausfeld, 2012), the analog of mammalian retinal ganglion cells (Solomon & Lennie, 2007). Early arthropods must have possessed highly developed color vision, as fossil evidence indicates early Cambrian arthropods had well developed homologous structures to the three main neuropils found in the vision pathway

of extant pancrustaceans (lamina, medulla, lobula and associated lobula plate shown in Figure i.2) (Ma, Hou, Edgecombe, & Strausfeld, 2012; Strausfeld, 2012).

It is puzzling that branchiopod crustaceans, unlike most other Pancrustaceans, possess only two main neuropils, for visual processing (lamina and lobula), as shown in Figure i.2A (Strausfeld, 2005). The medulla (2^{nd} optic neuropil), and the majority of the lobula complex (3^{rd} optic neuropil) have been secondarily lost or reduced in branchiopod crustaceans (Kress, Harzsch, & Dircksen, 2015; Ma, Edgecombe, Hou, Goral, & Strausfeld, 2015; Ma et al., 2012; Sinakevitch, Douglass, Scholtz, Loesel, & Strausfeld, 2003; Strausfeld, 2005). Despite lacking structures required for true color vision processing in other Pancrustaceans, the Anostracan and Notostracan branchiopods studied here express four and five opsins in their compound eyes, respectively (Henze & Oakley, 2015; Kashiyama et al., 2009).

Branchiopod Crustacean visual pathway **_D. melanogaster_ Color vision pathway**

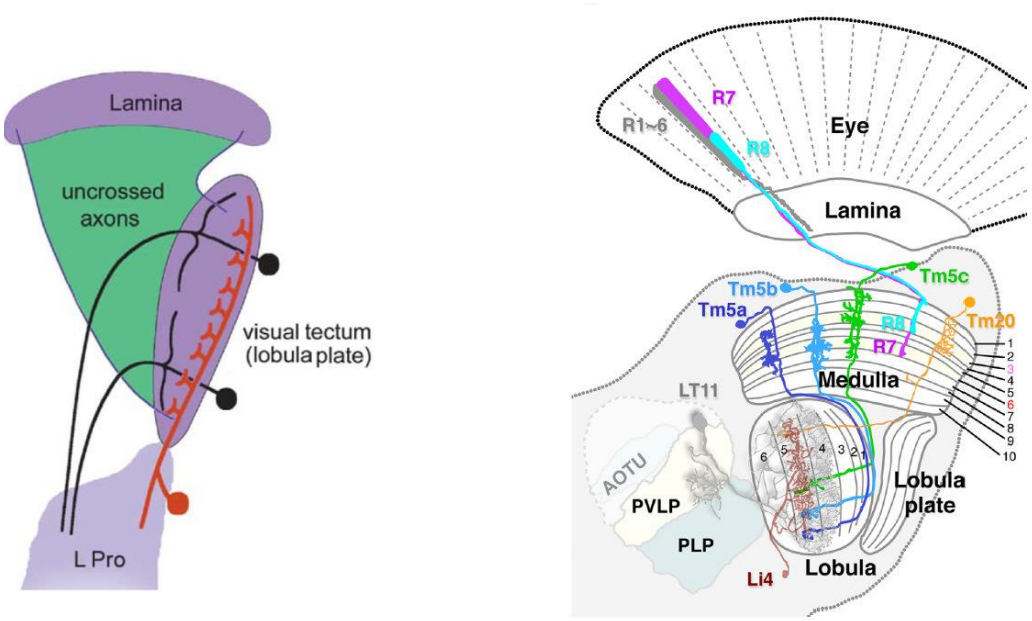

Figure i.2, after (Lin et al., 2016; Strausfeld, 2005)

Study System

I studied two representative species of branchiopods from separate orders that coexist in ephemeral pools throughout the arid Southwestern USA and Baja California, Mexico. *Triops longicaudatus* (Notostraca) is benthic, while *Streptocephalus mackini* (Anostraca) lives within the water column (Thorp & Covich, 2009). All branchiopod orders examined thus far possess multiple-pigment visual systems. *Triops* have been found to express the same five opsins in both its compound eyes and simple eyes, while members of Anostraca tend to express four opsins (Kashiyama et al., 2009). The representative of the best characterized branchiopod order, *Daphnia* (Cladocera) have been found by a variety of electrophysiological methods to use four spectral photoreceptor classes (Consi &

Macagno, 1985; K. C. Smith & Macagno, 1990). The chromophore (the light absorbing element in the visual pigment complex) for *Triops* is retinal (also known as A1). Knowing the identity of the choromophore allows the identification of the opsin (protein component) contribution to spectral sensitivity of a given visual pigment. Before the experiments reported here (Chapters 3) one Anostracan and Notostracan visual pigment was inferred to be UV sensitive due to similarities in the amino acid residue to other Pancrustacean taxa (Kashiyama et al., 2009).

Branchiopods are an ancient clade of crustaceans that are passive dispersers (Williams, 2005). They lay desiccation-resistant eggs which can remain in a resting phase for years (Thorp & Covich, 2009). These eggs require light and rehydration to resume development from the blastula stage, with only a percentage hatching in a given pool filling event as insurance against false starts (Brendonck, 1996). Notostracan and Anostracan resting-eggs hatch within 24-96 hours after an initial filling event (Fugate, 1992), with a peak in hatching in the first 24-48 hours (Fugate, 1992; Riley & Tsukimura, 1998). Predator cues have also been found to inhibit hatching of some branchiopods (Mayer, 2004).

Natural fish habitats in Southwestern North America consist of flowing streams (Minckley, 1973), and due to fish predation, Anostracans and Notostracans have been excluded from habitats that are fed by flowing streams (Dumont & Negrea, 2002. Therefore, Anostracans and Notostracans are found exclusively in temporary waters (Brendonck, Rogers, Olesen, Weeks, & Hoeh, 2008). Relegation to habitats which do not contain fish has taken place over evolutionary time scales, documented as large scale extinctions in the fossil record of Notostracan and Anostracan branchiopods in freshwater

habitats (Kerfoot & Lynch, 1987). The reason that temporary waters are of interest to visual ecologists is that their isolation and potential variation in optical properties provides an intriguing possibility for local adaptation.

Hypotheses and Tests

Based on the requirements for color vision I have addressed, the expression of multiple opsins in branchiopod visual systems suggest color vision, but the simplified neural systems of branchiopods suggest that they might have reduced color processing ability or unconventional vision, as summarized in Figure i.1. Because it was previously unknown how the opsins which are expressed in their visual systems contribute to spectral sensitivity for behavior, I proposed two main hypotheses:

(1) Branchiopod visual systems play a proximate role in the behavioral responses to light

Prediction: Branchiopods of both orders will respond to light over a broad spectrum to maintain vertical position in the water column and at dim intensities.

(2) There are physiological and morphological parameters which determine the information-gathering abilities of visual systems with multiple spectral classes, allowing modeling of the performance of their underlying light-sensitive structures

a. Branchiopods employ neural summation to maintain vision in the dim environments of temporary waters

Prediction: Modeling the minimum intensities based on histology of compound eyes and median eyes will indicate that receptors are summed from multiple compound eye ommatidia for behavior at dim intensities.

b. **Branchiopods use unconventional vision, in which multiple spectral photoreceptor classes contribute to retinal electrical responses that will mirror their behavioral responses across a range of wavelengths of light**

   Prediction: Electrophysiological responses from Notostracan and Anostracan branchiopods will indicate the spectral photoreceptor classes which are maintained in their compound eyes

c. **Because all animal visual systems use visual pigments as light sensitive molecules, spectral absorptance models will be applicable to visual systems with single spectral photoreceptor classes, as well as those with multiple spectral photoreceptor classes**

   Prediction: Multimodel selection techniques will infer the same spectral photoreceptor classes that have previously been empirically determined.

The studies described in the following chapters and appendices serve to test these hypotheses. I first describe the role of light for Anostracan and Notostracan branchiopods in regulating their preferred vertical position in the water column (Chapter 1). I then ask if at low light intensities, these branchiopods use neural summation from multiple compound eye ommatidia, or their median eyes, to gather information for behavior (Chapter 2). I then took electroretinographic recordings and modeled the spectral absorptance of their compound eyes and the first neuropil of their optic lobe, using multi-

model selection techniques to investigate whether branchiopods possess multiple spectral classes of photoreceptors. (Chapter 3). Finally, I use the multi-model selection method I developed for these branchiopods on a variety of spectral sensitivities of other organisms in order to determine if this modeling effort is widely applicable (Chapter 4). Together, these experiments identify whether Anostracans and Notostracans use unconventional vision to guide their behavioral responses to light.

CHAPTER 1

BEHAVIORAL RESPONSES INDICATE BRANCHIOPODS USE LIGHT TO MAINTAIN DEPTH IN THE WATER COLUMN

Introduction

Light is one of the primary environmental factors used by zooplankton for depth selection behavior (Cohen & Forward, 2009; De Meester, Dawidowicz, van Gool, & Loose, 1999). Early studies suggested that *Daphnia*, a suspension feeder, might use spectral preferences (termed "Color Dances") to regulate its vertical position toward alga-rich water (Lubbock, 1888; F. E. Smith & Baylor, 1953). However, recent studies have shown considerable regional spectral variation in shallow freshwater light environments, (Sabbah et al., 2011). Behavioral spectral responses correlated to light conditions suggest local preferences may depend on the regional light environment, rather than innate species-wide spectral preference associated with the transmission properties of algal chlorophyll (Stearns, 1975).

All branchiopod crustaceans, including tadpole and fairy shrimp, are passive dispersers, and are often found in hydrologically isolated, environmentally variable freshwater habitats (Brendonck et al., 2008; Williams, 2005). It is thought that a branchiopod selective history in variable environments, coupled with the temporary aspect of their habitats, has led to one of the highest levels of opsin gene duplication followed by evolutionary maintenance of animal genomes sequenced to date (Colbourne et al., 2011). Because opsin genes are one of the main genetic components of visual pigments, this indicates that branchiopods have had a selective history characterized by

opsin duplication, followed by changes to amino acid sequence structure which have been maintained by local adaptation. In this study, I sought to characterize Notostracan and Anostracan vertical position in the presence of downwelling light and gravitational cues, and then horizontal position in response to light cues alone.

Methods

Collecting site

Dry soil was collected from the upper 2.0 cm of the soil bank of an ephemeral pool community located in the Four Peaks Wilderness area in the Sonoran Desert (N 33.67005, W 111.46396). Multiple visits to the dry pool took place between 2011 and 2014. Resting eggs were collected in the soil samples. Soil was collected from throughout the catchment area of the dry pool (approximately 2000 m^2) and was mixed thoroughly within each sub-sample to avoid sampling soil which contained eggs from only a few individuals from the population. Reared animals were used because *S. mackini* lack a head-shield, making field-caught animals of this species difficult to catch and transport without damaging them. Adult *T. longicaudatus* can be caught in the field without damage using a dip-net, and this population has been tested to determine if the origin (field or lab) affects responses to light. Effect sizes for behavioral responses from this community are consistent for both greenhouse-reared (η_p^2= 0.470) and field-caught (η_p^2= 0.573) *T. longicaudatus*. Rearing conditions were established based on field measurements taken during seasonal monsoonal wet periods in 2012 and 2013 (maximum filled area 1,623 +/- 9 m^2, maximum depth of 17cm, and total suspended solids 0.40+/-0.23SD g/L).

Characterization of light environments

Natural ephemeral pool light environments depend on attenuation that occurs due to soil suspended in the water column. Suspended soil varies regionally due to soil particle size distribution (percentages of sand/silt/clay) affecting the total number of particles suspended in the water column, as well as particle-specific transmittance properties (Partridge & Cummings, 1999).

To describe the spectral properties of ephemeral pool light environments with increasing depth, I took calibrated light measurements of downwelling irradiance during seasonal monsoonal wet periods. Downwelling irradiance (Figure 1) was measured in the field at 1.0 cm intervals from just below the surface, every three days from time of filling in six ephemeral pool communities (100 m^2 or greater), between 10:00 and 14:00. Measurements were taken using a USB 2000+ spectrometer (Ocean Optics; Dunedin, FL), 10m optical fiber of 400 μm diameter, and CR2-OR 0.635 cm diameter waterproof cosine corrector (Stellarnet) with a spectroradiometric calibration from Ocean Optics Inc. In order to characterize each light measurement with a single value, the wavelength at which half the total number of photons between 300 and 700nm, λ_{P50}, was calculated. This parameter has been used to describe other bodies of shallow water (Sabbah et al., 2011).

Rearing procedures

Animals used in this study were reared in wading pools (1.0 m diameter) within a greenhouse facility under natural sunlight (Appendix A). Wading pools were each filled

with 80 L of deionized water, and then 1.5 L of collected soil was mixed into the water. After 24 hours, an additional 20L of deionized water was added, and the water level was maintained at 100L at a depth of 11.5cm in the center of each wading pool. Temperatures were maintained on a 25:15 C diel temperature cycle in the greenhouse. Animals developed brood pouches within 5-7 days after hydration of resting eggs, as observed in the field. No food supplement was added until animals with brood pouches were observed because the majority of larval food is contained in the soil (Centeno, Brendonck, & Persoone, 1993). After adult animals were observed, 10 mL of 0.025g/mL Brewer's yeast solution (Twinlab, Inc), was stirred into the water in each wading pool once a week.

In order to verify the species of reared animals, DNA was extracted and a COI mitochondrial segment (Folmer, Black, Hoeh, Lutz, & Vrijenhoek, 1994) was amplified from 20 individuals used in behavioral trials, verifying species as *T. longicaudatus* and *S. mackini*. *T. longicaudatus* from this population consist only of self-fertilizing hermaphrodites (Maeda-Martinez, Belk, Obregon, & Dumont, 1997), verified using the presence of brood pouches of each individual. *S. mackini* are gonochoristic, meaning they have separate sexes. Individuals of each sex were identified using the presence/absence of brood pouches and second antennal appendages (Belk, 1975).

Vertical distribution and sinking controls

To assess depth preferences in the presence of gravitational and visual cues, a cylindrical glass testing column was marked into 5 horizontal sections of 4cm each. It was used for testing in both a greenhouse setting under broad spectrum light including

UV (Appendix A), and for controls in a darkroom. Testing groups included 10 shrimp in each trial, with groups of *S. mackini* consisting of either 10 males, 10 females or 5 males and 5 females. The testing column was placed in the center of a square cardboard foundation on top of a freestanding table in a greenhouse setting. The foundation had walls which limited the view of the surroundings. A removable frame was placed above the apparatus during testing and parchment paper served as a broad-band diffuser of downwelling greenhouse light (Appendix A). The testing apparatus (walls, foundation and the exterior of the base of the column were spray-painted flat black.

S. mackini were sexed and separated into groups at the beginning of each day of testing, and all shrimp were acclimated in deionized water for 3 hours prior to testing. Testing took place in a greenhouse between 10:00-14:30. Six trials of 36 minutes each were carried out on each testing day, and the testing group order was alternated on each day to avoid order effects with time of testing. Between trials, the water was removed, and the column was cleaned. 12 replicates were carried out for each group composition for *S. mackini* and 10 replicates for *T. longicaudatus*. At the beginning of a trial, a testing group was gently pipetted into the vertical column. Testing was only carried out on cloudless days. Downwelling light levels at the apex of the testing column were measured at 14:00 on a cloudless day, with the same equipment used for field measurements (Appendix A).

Video recordings in the greenhouse were taken using a SDR-S7 digital video camera (Panasonic; Panasonic Corporation, Secaucus, NJ), with its lens positioned to view the column through a 4 cm diameter opening in the apparatus. Video recordings were taken in the darkroom using a C5900 H.264 wireless IP camera (Esky; Hong Kong)

with a built-in infrared light source (>800nm) for illumination during recording that is unlikely to be detected by the test animals (see Chapter 3). Shrimp were observed on the camera screen or remotely from the laptop during testing, and the numbers of dead or non-responsive fairy shrimp were recorded every 12 minutes during testing. Shrimp were assessed as non-responsive if they ceased gill-beating activity and did not move at all between subsequent 1-minute intervals.

To quantify depth preferences we extracted individual frames from the end of each 1 minute interval using VLC media player (VideoLAN). The first minute interval was not included in analyses as shrimp often displayed an initial flight reaction and then resumed regular swimming. Video files from each trial were assigned a randomized accession number, and each frame was scored manually. The scorer was blind to the group composition and it was not possible to resolve sexual characteristics in the extracted frames. Based on preliminary results, experimental trials were stopped after 36 minutes of continuous video from the time that shrimp were released in the column, to ensure only active animals were being tested. To avoid pseudoreplication from each trial, the 10^{th} frame was compared among replicates. A two-way Chi-square test determined if the frequencies of animals in each vertical section was dependent on group composition, and if greenhouse experiments differed from darkroom controls. A subsequent Hochberg sequential Bonferroni correction (Hochberg, 1988) was used to determine which vertical sections differed for each group composition or greenhouse/darkroom treatment.

A control experiment was carried out to compare sinking speeds of anesthetized shrimp which were not swimming. Shrimp were placed in carbonated water for 3 seconds, after which no gill-swimming was observed. Shrimp were then individually

spooned into the testing column and the time to sink to the bottom of the column was recorded with a stopwatch to determine an average sinking rate.

Horizontal responses to narrow bandwidth stimuli:

To determine whether there were interactions of wavelength and intensity in the absence of gravitational cues, we quantified a behavioral response index to narrow spectral bandwidth stimuli in the horizontal plane using an acrylic chamber with sliding dividers and illumination from one end following testing procedures described in (Cohen et al., 2010). Testing took place between 9:00-16:00. Animals which were to be tested were first netted or pipetted in the greenhouse, and then allowed to dark-acclimate for at least 1 hr in aerated deionized water in the darkroom before testing. A Plexiglas trough (40x10x10cm) divided into five equal longitudinal sections was used. The testing trough was placed 55 cm from the light source, which provided even illumination along its longer axis. Sections were separated by dividers which could be removed and then replaced in unison.

Each trial consisted of filling the trough with 2.0 liters of aerated deionized water, placing 8 animals in the center compartment, giving them 30 seconds to acclimate. The light source (Viewlex film projector; 500W Sylvania CZX/DAB tungsten bulb), and cooling fan were then turned on, the dividers were removed, and animals were allowed to move freely for 45 seconds. The lowest photon flux experienced by animals in the middle section of the trough was controlled to be $10^{3.5}$ photons/cm^2/sec, at all wavelengths tested (Appendix A). Each group was tested four times using two log unit intervals of increasing photon flux, starting at $10^{3.5}$photons/cm^2/sec. In control trials, only the cooling

fan was turned on. Infrared radiation from the light source was limited using a hot mirror (Edmund Optics; Barrington, New Jersey) and was not detected in irradiance measurements taken after the lamp was left on for a six hour testing period. Stimuli were manipulated using interference filters with a bandwidth at half maximum of 12.5nm (Edmund Optics; Barrington, New Jersey), with center wavelengths ranging from 410 to 636nm. Irradiance was controlled using neutral density filters (Edmund Optics; Barrington, New Jersey) and was measured in the position of the center chamber using the calibrated spectroradiometer described for field measurements.

The dividers were then replaced and the numbers of animals in each chamber were counted, with the number found in the two chambers nearer the light source scored as "towards", and those found in the chambers further from the light source counted as "away". Between experimental trials, animals were allowed to acclimate in the central division for 5 minutes. After the final experimental condition at $10^{9.5}$photons/cm^2/sec, the same individuals were tested once more under dark conditions to ensure no trail following occurred and that animals remained behaviorally responsive. Each group of animals was tested at only one wavelength or under repeated control conditions only. Between trials of increasing irradiance, animals were carefully removed and the clear Plexiglas trough was rinsed out to eliminate the possibility of trail-following.

I further calculated a response index for each horizontal trial to create a single response metric ranging from -1 to 1:

$$R_{ind} = \frac{\#Towards - \#Away}{\#Total}, \quad (1)$$

Where "#Towards" is the number of animals that moved towards the light, and "#Away" is the number that moved away.

Results

Light environments of ephemeral pools

The spectral quality (λ_{P50}, the wavelength at which 50% of photon flux distribution) of ephemeral desert pools varies considerably due to the effects of suspended soil (Chapter 3), with a spatial coefficient of variation of 11.8% among all habitats (N=6), and a temporal coefficient of variation of 3.9% within habitats. λ_{P50} of the ephemeral pool habitat corresponding to animals used in this study was 534nm (Figure 1, dark gray). Depths of these habitats varied from 10.0cm to 132.0cm, and the total area for each habitat was >100m^2 after initial filling. In order to compare among all pools, λ_{P50} is compared at a depth of 5.0cm (Figure 1).

Variation and behavioral distribution in the water column

S. mackini tended to swim in the water column in the greenhouse and were more likely to maintain a lower position in the dark (Figure 2B, asterisks). I found the vertical distribution of *S. mackini* to depend on group composition (Figure 2A, Chi-square test of independence, χ^2=19.13, *P*=0.014, *N*=257). Males were more likely to maintain a vertical position of 12.0-16.0 cm above the substrate than females, whether females were present or not (Figure 2A, asterisks). *T. longicaudatus* tended to maintain a vertical position between 0-4.0cm from the substrate in greenhouse light conditions, with more sporadic movements towards the surface under dark conditions (Figure 2B, Chi-square test of independence, χ2=22.96, P=0.004, N=187). To further assess if shrimp actively maintained a vertical position, we measured the sinking rates of anesthetized shrimp (Figure 2C), indicating male *S. mackini* sink faster than females (One-way ANOVA

followed by Tukey's post hoc test $F_{2,40}=24.20$, $p<0.01$), yet males tended to swim slightly above females in the greenhouse experiments (Figure 2A).

Behavioral response index

T. longicaudatus moved away from all tested wavelengths, and all intensities of $10^{5.5}$ photons/cm^2/sec or greater (Figure 3A,B). To determine if *S. mackini* displayed sex-specific behavioral differences, we tested each sex in separate experiments. Both male and female *S. mackini* moved away from light at intensities above $10^{5.5}$ photons/cm^2/sec. At intensities of $10^{5.5}$ photons/cm^2/sec, I found that *S. mackini* males moved towards light of 532 nm (Figure 3C), with the narrow bandwidth suggesting the use of a single class of spectral photoreceptor with an absorptance peak near this waveband. Female *S. mackini* did not move towards light at any of the tested wavelengths and intensities (Figure 3D). The minimum response intensities for both species of branchiopods (Figure 3A-D) are lower than those of starlight in a terrestrial habitat (Chapter 2).

Discussion

My results suggest that both species of branchiopods use downwelling light to behaviorally regulate their position in the water column. The broad spectral bandwidth of behavioral responses (Figure 3B-3D) suggests both *T. longicaudatus* and *S. mackini* employ multiple spectral photoreceptor classes to position themselves vertically in the water column. *Triops longicaudatus* and *Streptocephalus mackini* are found in temporary waters throughout arid Southwestern North America, and have been previously been described as benthic and living within the water column, respectively (Thorp & Covich,

2009). The results presented here support these characterizations of their respective microhabitats in the water column, and further indicate that behavioral responses to light are involved in maintaining them.

Interestingly, at intensities of $10^{5.5}$ photons/cm^2/sec, I found that *S. mackini* males moved towards light of 532 nm (Figure 3C) and because male *S. mackini* behavioral responses were dependent upon intensity, I refer to this behavior as wavelength-specific (Goldsmith, 1990; Kelber & Osorio, 2010). The narrow bandwidth of male positive responses at 532nm suggests the use of a single class of spectral photoreceptor with an absorptance peak near this waveband. Further, this waveband very closely matches the specific light environment of the habitat from which the animals were reared, characterized by λ_{P50} of 534nm. Because male *S. mackini* tended to swim higher than females in the water column when light cues were available, whether females were present or not, males most likely use vision to maintain their vertical position at a higher position than females. However, further studies would be needed to determine whether courtship behavior involves vision as well as other sensory modalities, such as those of other Anostracans (Belk & Martin, 1991).

The findings presented in this chapter indicate that light environments in these pools are spectrally variable, and that branchiopods may use multiple spectral photoreceptor classes to broaden the spectral sensitivity of their behavioral responses. Therefore, I suggest that behavior which is mainly guided by luminance vision from multiple spectral photoreceptor classes is possible. These findings are explored further in Chapter 3.

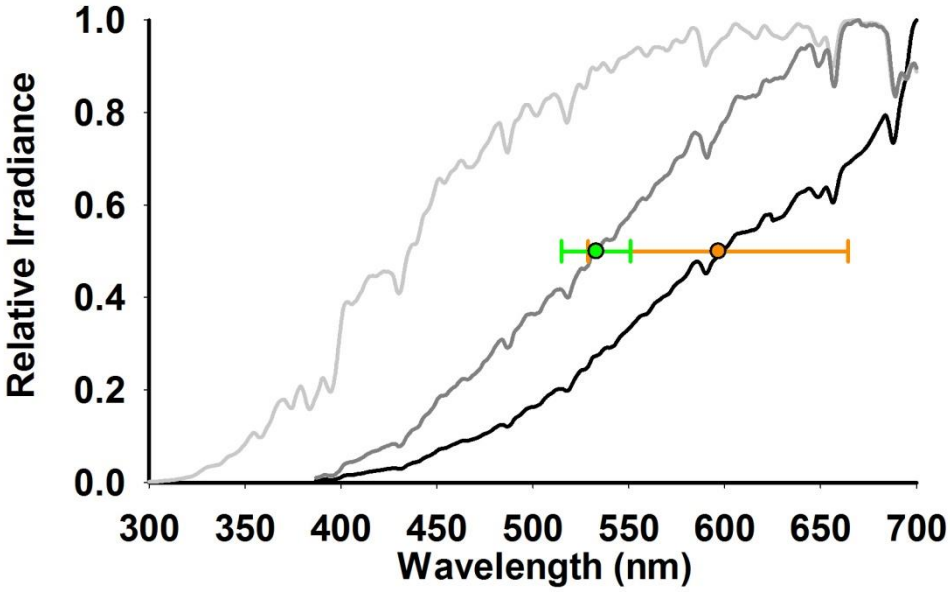

Figure 1. Environmental Light Variation in Shallow Freshwater Habitats. Relative averaged downwelling irradiance at 0cm, just below the surface (light gray) and at 5 cm depth (dark gray) for the ephemeral pool community for this study (N=9) and at 5 cm depth (black) for six ephemeral pool habitats ephemeral freshwater habitats greater than 100 m^2in Arizona, USA, measured between 10:00 and 14:00 on cloudless days (N=86). The green and orange circles indicate the wavelength at which 50% of the photon flux distribution occurs (λ_{P50} +/- SD) at 5cm (not shown for surface measurements). Measurements were taken every three days from initial filling of six ephemeral pool communities, throughout the life history of branchiopod inhabitants in the field. Irradiances were each standardized relative to peak photon flux of each measurement from 300-700nm.

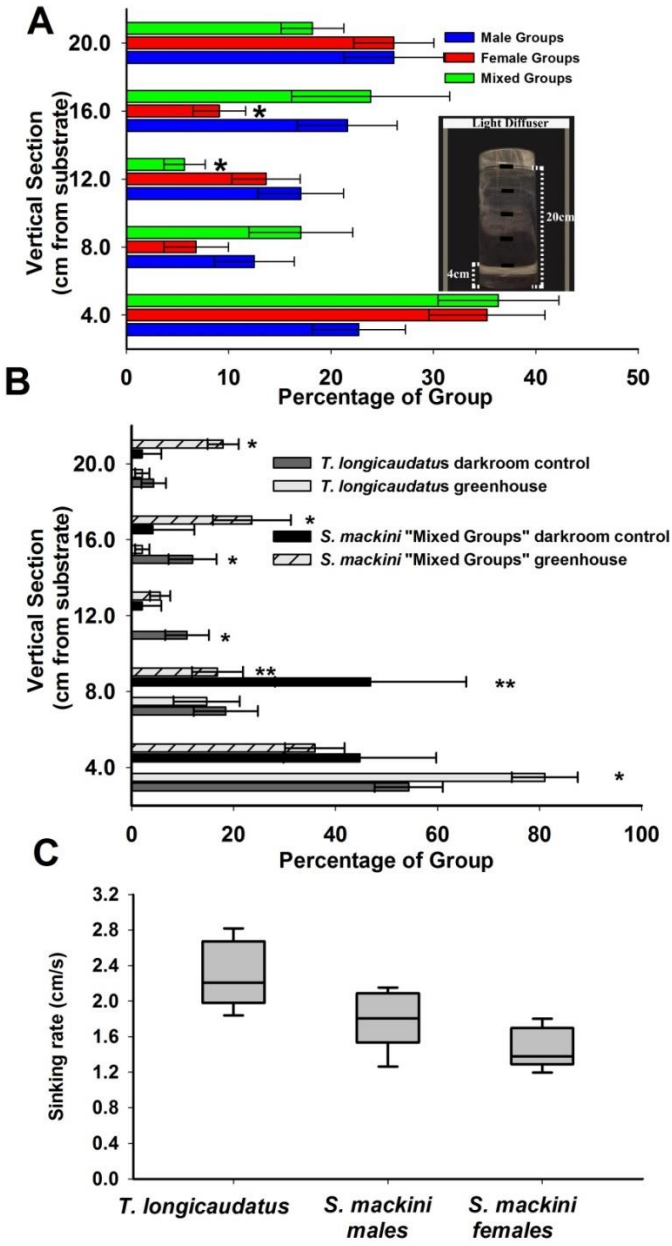

Figure 2. Behavioral Distribution in the Water Column. (A) *S. mackini* vertical distribution under diffuse, broad-spectrum light in the greenhouse (n=120 individuals for males, females, and mixed groups). "Mixed Groups" contained 5 males and 5 females in each trial. Bonferroni-corrected test significance at each position is indicated at $p < 0.05$ by asterisks. (B) Comparisons between vertical distributions in greenhouse light environment (light gray) and darkroom control tests (dark gray) for *Triops longicaudatus* (solid fill) and *Streptocephalus mackini* (striped fill). *S. mackini* N=205, *T. longicaudatus* N=187. Error bars indicate SEM. Bonferroni-corrected significance at each position is indicated at $p < 0.05$ by a single asterisk, and at $p < 0.01$ with two asterisks. (C) Mean sinking rates of anesthetized *T. longicaudatus* (n=12) and *S. mackini* ♂ (n=13) *S. mackini* ♀ (n=15). Whiskers indicate 95% confidence intervals.

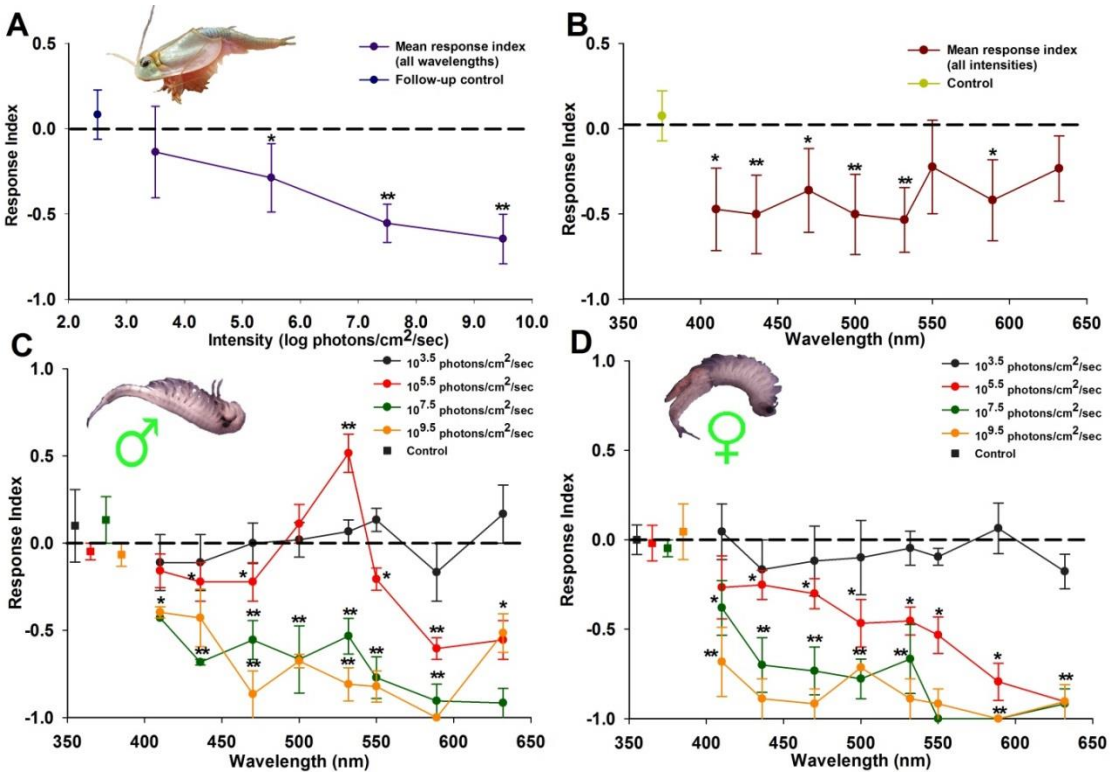

Figure 3. Behavioral Response Index for Dark-acclimated Branchiopods.
(A and B) *T. longicaudatus.* As there was no significant interaction $F(32,72) = 0.702$, $p = 0.865$, data are presented as marginal means +/- SEM, across all tested wavelengths (A), and across all tested intensities (B) . Main effects of wavelength (Between Subject factor) and intensity (Within Subject factor) were significant. [Mixed ANOVA, Between Subjects Factor $F(8,18) = 3.67$, $p = 0.010$, Within Subjects factor $F(4,72) = 15.99$, $p < 0.0001$].
(C) *S. mackini* males. There was a significant effect of interaction $F(32,72) = 4.465$, $p < 0.0001$). Main effects of wavelength (Between Subject factor) and intensity (Within Subject factor) were significant. [Mixed ANOVA, Between Subjects Factor F(8,18) = 5.611, p = 0.001, Within Subjects factor F(4,72) = 76.29, p <0.0001].
(D) *S. mackini* females. There was a significant effect of interaction F(32,72) = 1.704, p = 0.032). Main effects of wavelength (Between Subject factor) and intensity (Within Subject factor) were significant. [Mixed ANOVA, Between Subjects Factor $F(4,72) = 8.817$, $p < 0.0001$, Within Subjects factor $F(4,72) = 64.445$, $p < 0.0001$].
Post hoc test significance is indicated at $p < 0.05$ by a single asterisk, at $p < 0.01$ with two asterisks. Main effects with Bonferroni correction in (A and B), and Two-way Dunnett's test versus control in (C and D). (n=24 individuals for each wavelength/intensity)

CHAPTER 2

BRANCHIOPODS USE NEURAL SUMMATION TO MAINTAIN VISION IN THE DIM ENVIRONMENTS OF TEMPORARY WATERS

Introduction

In order to acquire information in dim environments, many organisms employ neural summation, in which either spatial, or temporal summation provides an increased signal to noise ratio by using neural pathways which incorporate electrical signals integrated from multiple optical units, or over time (Bradbury & Vehrencamp, 1998). Insects and crustaceans are well known to incorporate spatial summation in the first neuropil of their compound eye optic lobe, the lamina (Preface Figure i.2) (Warrant, 2005). This form of summation comes at a tradeoff between sensitivity, and resolution, which is why organisms living in higher intensity environments do not employ neural summation (Land & Nilsson, 2012).

Light attenuates quickly with depth in many shallow freshwater habitats (Jerlov, 1968). In this study, I sought to describe how in ephemeral pools light attenuates with depth, and to infer whether Notostracans and Anostracans use neural summation from their compound eye ommatidia, or their median eyes, to gather information which was used for the depth preference behavior at dim intensities described in Chapter 1.

Methods

Downwelling attenuation

Measurements were taken using a USB 2000+ spectrometer (Ocean Optics), 10m optical fiber of 400 μm diameter, and CR2-OR 0.635 cm diameter waterproof cosine corrector (Stellarnet) with a spectroradiometric calibration from Ocean Optics Inc. Localized diffuse spectral attenuation coefficients, at a centimeter scale, are presented in 10nm bins, and are shown in Figure 4 and Appendix B for comparison to other aquatic environments (Jerlov, 1976). Attenuation coefficients were calculated by dividing the photon flux measured just below the surface, and dividing this by the photon flux at a depth of 1.0cm. Note that the clearest waters transmit the most light at 474nm, which is not the case for coastal marine environments (Figure 4B).

Modeling minimum response intensity I_{min}

We modeled the minimum response intensity (see Appendix C for development of these equations) that each species would be able to detect in behavioral trials from their median eyes:

$$I_{min} = \frac{N_{min}}{2\pi\left(1-\cos\frac{\Delta\rho_m}{2}\right)\pi\left(\frac{D_m}{2}\right)^2\kappa\tau\left(\frac{kl}{2.3+kl}\right)\Delta t}, \quad (2a)$$

and from their apposition compound eyes:

$$I_{min} = \frac{N_{min}}{1.269\left(\frac{\Delta\rho_{sum}}{\Delta\phi}\right)^2\Delta\rho_c^2 {D_c}^2\kappa\tau\left(\frac{kl}{2.3+kl}\right)\Delta t}, \quad (2b)$$

$$\boldsymbol{\Delta}\rho_{sum} = \sqrt{\left(\frac{4n_c\delta C}{\pi}\right)}, \quad (2c)$$

where $\Delta\rho_m$ is the angle of the apex of the detected cone of light for median eyes in radians, $\Delta\rho_c$ is the acceptance angle of a single ommatidium, D_m is the diameter of the median eye, D_c is the diameter of the branchiopod crystalline cone, κ is the quantum

efficiency of transduction, τ is the transmission of eye media, k is the photoreceptor absorption coefficient, Δt is the integration time of the photoreceptor, l is photoreceptor length. $\Delta\rho_{sum}$ is the estimated angular output from neural spatial summation, $\Delta\phi$ is the interommatidial angle, n_c is the number of contributing optic cartridges in the lamina, δ is the solid angle viewed by a single cartridge, and C is the packing ratio of monopolar cells to optic cartridges. The term $\frac{kl}{2.3+kl}$, is a correction for the underlying assumption that k is at peak absorbance for a visual pigment, which is not possible at all wavelengths (Warrant & Nilsson, 1998). N_{min} is the minimum photon sample needed to evoke a response overcoming photon shot noise, $\sqrt{N}$. Values used for these parameters are found in Table 1, with considerations for neural summation in the lamina explained in Appendix C . Note that Equation 2a and 2b are fundamentally similar and are developed in the Appendix C. Equation 2a was developed from (Nilsson, 2013) in radians and equation 2b and 2c from (Theobald, Greiner, Wcislo, & Warrant, 2006; Warrant, 1999), in degrees.

Histology

To measure photoreceptor lengths for use in equations 2a and 2b, I carried out histology and light microscopy techniques on fixed and embedded animals. Shrimp which were not used for electrophysiology experiments (n=4), were dark-acclimated for at least 1hr. Their heads were dissected, fixed, dehydrated in an ethyl alcohol series, and infiltration using LR White resin (Electron Microscopy Sciences; Hatfield, PA). Heads were placed in 1mL gelatin capsules with LR White and polymerized at 60°C for 24 h.

Resin blocks were then sectioned at a thickness of 1.0μm using an Ultracut R microtome (Leica; Wetzlar, Germany), and stained using 1% toluidine blue. Compound eye parameters were inferred using light microscopy from multiple sections of four individuals for each species or sex. Images were taken of sections and a calibration slide using an ocular Optixcam 5.0 MP digital camera, and were later measured using Image J software (National Institute of Health). More specifically, total photoreceptor (rhabdom) lengths, rhabdom width, and local radius of curvature and crystalline cone width were measured from these sections using Image J. These parameters were used to calculate $\Delta\rho_c$, and $\Delta\varphi$.

Results

Ephemeral desert pool habitats at depths of less than a meter tend to have light intensities lower than those of terrestrial habitats under dim starlight (Figure 4). In comparison to other aquatic habitats, light attenuation per centimeter in the water column is approximately two orders of magnitude higher than the most heavily attenuating coastal waters on the Jerlov scale (Figure 4B). We modeled the minimum intensity (I_{min}) required to elicit a detectable response from branchiopod median eyes in comparison to compound eyes which employ neural summation in the lamina of the optic lobe (Table 1). I_{min} for compound eyes which incorporate summation are approximately one order of magnitude lower than in median eyes for both species. I_{min} from median eyes is approximately one order of magnitude higher than the dimmest intensities for behavior described in Chapter 1. We did not find sex-specific differences in I_{min} for *S. mackini* (Table 1). Although I_{min} is in steradians, we measured our intensities as irradiance for

behavior in Chapter 1 using a cosine-corrected probe. However, the light projected on the horizontal testing chamber was set up so that it provided a even gradient along its length. Under such diffuse illumination, with an apex angle of approximately 180 degrees, the difference between radiance and irradiance is a factor of π, and if I_{min} were converted to irradiance, it would lead to lower I_{min} values for both compound eyes and median eyes, with median eyes still not able to detect starlight intensities.

Discussion

As I have described, light in ephemeral pool habitats attenuates rapidly with depth. It follows that organisms in these habitats will experience selective pressures which favor photoreception in dim environments, or the evolutionary loss of visual organs, as occurs repeatedly in crustacean cave species (Protas, Trontelj, & Patel, 2011). The intensities I have modeled (Table 1) indicate that neural summation from multiple compound eye ommatidia is responsible for behavior at dim intensity from multiple spectral classes of photoreceptor described in Chapter 1 (Figure 3).

The occurrence of neural summation in these animals is of interest for two reasons. First, the first neuropil of the optic lobe of crustaceans and insects contain large monopolar (LMC) cells that pool responses from multiple ommatidia via lamina amacrine neurons, also found in branchiopods (Figure 5C, D) (Nässel, Elofsson, & Odselius, 1978; Sims & Macagno, 1985; Sinakevitch et al., 2003; Strausfeld, 2005). Such laminar circuits are responsible for the summation of multiple photoreceptor spectral classes for achromatic visual behavior at low intensity in honeybees (Menzel & Greggers, 1985), and are required to achieve predicted I_{min} in our modeling of branchiopod

compound eyes (Table 1). Branchiopods must employ laminar summation from multiple ommatidia in order to respond behaviorally at the intensities described here.

Second, chromatic discrimination in crustaceans and insects is enhanced by the segregation of photoreceptor spectral channels with long visual fibers that penetrate the lamina (Kelber & Henze, 2013). For *Drosophila melanogaster* spectral preference behavior at low intensity, this segregation is maintained via an amacrine medulla neuron which effectively sums the signal of a single spectral photoreceptor class with long visual fibers from multiple ommatidia (Gao et al., 2008). Photoreceptors with longer visual fibers are lacking in Notostracans (Figure 5C), (Sinakevitch et al., 2003), and we find no evidence of wavelength specific behavior in *T. longicaudatus* due to the lack of a significant interaction of wavelength and intensity (Chapter 1 Figure 3A,B). Photoreceptors that terminate at two separate strata in the lamina are found in Anostracans (Kress et al., 2015; Nässel et al., 1978; Strausfeld, 2005). However, in order for spectral discrimination via opponent processing to occur at the dimmest response intensities for *S. mackini* wavelength-specific behavior, the neural signal would need to be compared synaptically after pooling within spectral classes from multiple ommatidia as for *Deilephila elpenor,* (Kelber et al., 2002). Given the optical limits of apposition eyes and neural summation we have modeled in the lamina, it is very unlikely color vision is used at the intensities at which we describe behavioral responses.

The minimum response intensities we have described for both species of branchiopods in Chapter 1 fall below those of starlight in a terrestrial habitat (Figure 4). Unlike the nocturnal hawkmoth, *Deilephila elpenor*, which uses superposition compound eyes for color vision under dim starlight intensities (Kelber et al., 2002), Anostracans

(Elofsson & Odselius, 1975), and Notostracans (Diersch, Melzer, & Smola, 1999) have apposition compound eyes. Such eyes are generally found in diurnal invertebrates that live under high light intensity conditions. However, neural summation has been found in insects with apposition eyes that are nocturnal (Warrant et al., 2004), and even for color vision under starlight conditions (Somanathan, Borges, Warrant, & Kelber, 2008).

The modeling results of Chapter 2 suggest that both species of branchiopods use their compound eyes to respond behaviorally to light of dim intensities found in their habitats. Chapter 1 indicated that branchiopod behavior is guided by more than one spectral class of photoreceptor. In order to assess whether the branchiopods studied here use unconventional vision, and the properties of the spectral photoreceptor classes which are summed, in Chapter 3, I use electroretinography and multi-model selection to infer the number of spectral classes that are found in their compound eyes.

Table 1. Parameters Used to Model I_{min}, incorporating Equations [2a], [2b], and [2c]. from text, which are developed in Appendix C. Values used for k here were established by (Bruno, Barnes, & Goldsmith, 1977) and are typical for other crustaceans and insects (Cronin, Johnsen, Marshall, & Warrant, 2014b). For apposition compound eyes of branchiopods, which have a single lens for each ommatidium formed by their crystalline cones, neural summation was incorporated using eq. [2c] to estimate an angular output channel $\Delta\rho_{sum}$, formed by the summation of N_c optical cartridges shown in Figure 5C and D). D_c, $\Delta\rho_c$, and $\Delta\phi$ were estimated from measurements taken using digital photos of 1.0 μm sections and a calibration slide, in Image J. Note that I_{min} is determined primarily by D, the diameter of the light gathering structure, and $\Delta\rho$. I use conservative estimates from ref.(Nilsson, 2013) indicated by an asterisk (*) for N quanta needed to achieve intensity discrimination, and a longer integration time for median eyes, supported by (Laughlin, 1981). Parameters for a theoretical median eye ref.(Nilsson, 2013) and the superposition compound eye of the hawkmoth *Deilephila elpenor* (Kelber et al., 2002) are included for reference. I calculated I_{min} for *D. elpenor* using equation [3a] from the main text because the relevant aperture is of a superposition eye, in which ~568 facets each contribute to a single effective lens.

Species/sex and eye type	I_{min} (photons/ cm^2/sec/sr)	D_m or D_c (µm)	l (µm)	Δt (s)	N_{min} (quanta)	$\Delta\rho_m$ or $\Delta\rho_c$ (degrees)	k $_{x10^{-3}}$	N_c Number of lamina cartridges
Triops longicaudatus apposition compound eye	8.01 x10^5	52.1	142	0.05*	100*	17.1	0.8	11
Triops longicaudatus median eyes	3.65x10^6	244	25*	0.5*	100*	180*	0.8	-
Streptocephalus mackini apposition compound eye	7.95x10^5♂ 6.55x10^5♀	33.7♂ 34.3♀	136♂ 129 ♀	0.05* 0.05*	100*	9.4 10.1	0.8 0.8	14 14
Streptocephalus mackini median eyes based on ref.(Elofsson, 1966) for related *Branchinecta paludosa*	6.46x10^6	140	25*	0.5*	100*	180*	0.8	-
Theoretical (median eye) for directional behavior such as swimming phototaxis. Parameters from (Nilsson, 2013)	3.16x$10^{8.5}$ = 12.5 log photons/m^2/sec)	10*	500*	1.0*	100*	180*	1*	-
D. elpenor superposition compound eye from parameters used in (Kelber et al., 2002)	1.18x10^6 = dim starlight	27µm x 568 facets	414	0.036	15	3	0.67	-

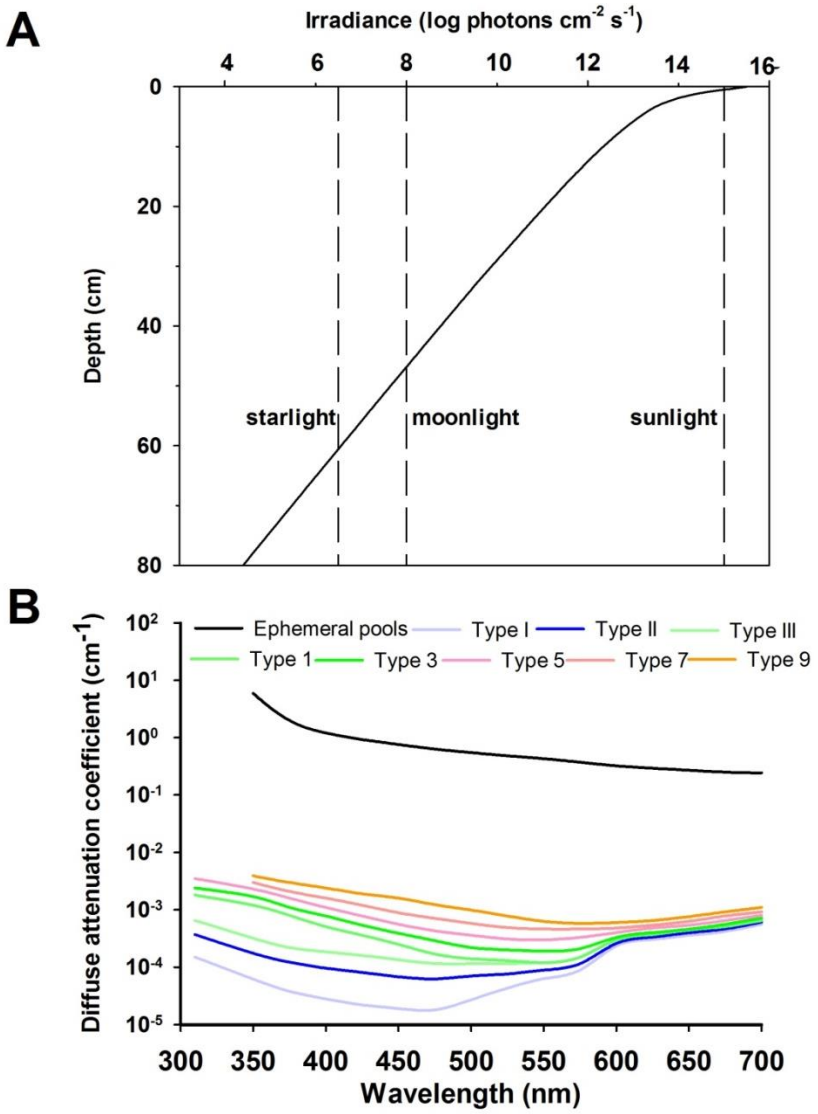

Figure 4. Intensity Loss With Depth in Ephemeral Pools of Arizona, USA.
(A) Comparison of modeled intensity loss as a function of depth (in centimeters) in ephemeral freshwater habitats of Arizona, USA. Dashed reference lines are included for comparison to light levels of terrestrial habitats, and represent sunlight, moonlight (full moon), and starlight under clear conditions. Downwelling irradiances were modeled at (λ_{P50} +/- SD) for each measurement.
(B) Diffuse attenuation coefficients of downward irradiance, shown here for comparison to other bodies of water using the Jerlov Scale (Jerlov, 1976). The black line presents attenuation coefficients at 1.0cm for ephemeral pools in Arizona (N=86), measured at 1nm intervals, binned here to 25 nm intervals for comparison with values reproduced from (Jerlov, 1976). Note that (Jerlov, 1976) use attenuation in the upper 10 meters of the water column, interpolated here to 1cm. The bodies of water range from the least-

attenuating (Jerlov Type I, light gray) to coastal and heavily attenuating (Jerlov Type 9, orange).

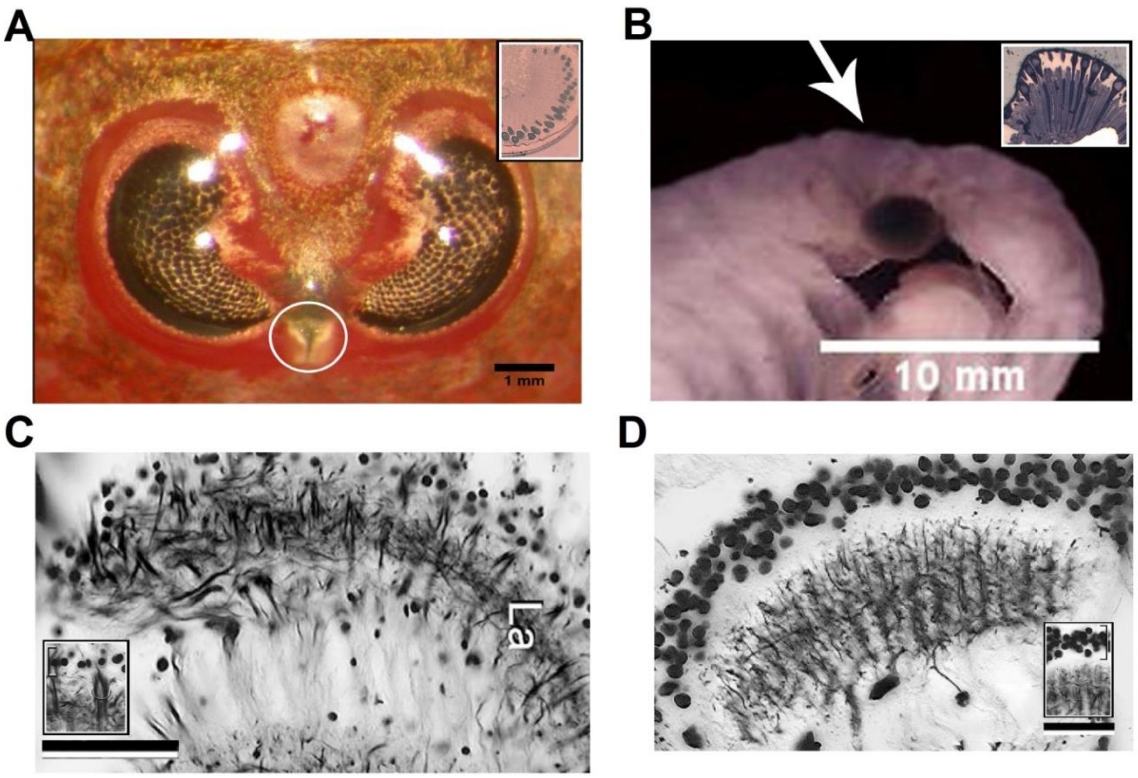

Figure 5. Histological Parameters of Compound Eye Laminar Neural Summation. (A) *T. longicaudatus* compound eyes , with the median eye indicated by a white circle. Insets show representative semi-thin histological sections of their compound eyes used to estimate modeling parameters (Table 2). (B) *S. mackini* compound eye and median eye location marked with an arrow. (C,D) Notostracan and Anotostracan laminas, after (Strausfeld, 2005). Insets show the ratio of monopolar cells (brackets) to optic cartridges, estimated by(Strausfeld, 2005) to be 6.3:1 for Anostracans, and 3:1 for Notostracans, and used as parameter C in Equation 3C of this supplement. The number of effective optic cartridges was also estimated from these images for parameter N_c in equation 3C (Table 2). Scale bars =25 μm.

CHAPTER 3

BRANCHIOPODS USE UNCONVENTIONAL VISION

Introduction

Many animals possess multiple spectral classes of photoreceptors that determine the spectral information which can be gathered to guide behavior (Kelber & Osorio, 2010). Behavior which results from true color vision is largely independent from stimulus intensity due to opponent processing between spectral channels via synaptic connections (Menzel, 1979). However, behavioral evidence may indicate that animals which possess multiple photoreceptor classes do not use all of them for true color vision. When such behavioral evidence is available, it indicates that these animals have unconventional color vision (Marshall & Arikawa, 2014; Thoen, How, Chiou, & Marshall, 2014; Wakakuwa, Stavenga, & Arikawa, 2007), a broader category that includes wavelength-specific behavior which is dependent upon intensity from a subset of photoreceptors (Cohen et al., 2010; Kolb & Scherer, 1982; Menzel & Backhaus, 1991). In Pancrustaceans, a group of arthropods composed of hexapods and crustaceans, the synaptic connections used for color comparisons are found mainly in the medulla of the optic lobe (Dyer et al., 2011; Kleinlogel et al., 2003; Melnattur et al., 2014; Morante & Desplan, 2008; Paulk et al., 2009; Strausfeld, 2012), the analog of mammalian retinal ganglion cells (Solomon & Lennie, 2007). Because the medulla has been secondarily reduced in branchiopod crustaceans (Kress et al., 2015; Ma et al., 2015, 2012; Sinakevitch et al., 2003; Strausfeld, 2005), I explored the possibility that two species of branchiopods, *Streptocephalus mackini* (Order Anostraca), and *Triops longicaudatus* (Order Notostraca) use information

from multiple spectral channels to guide behavior that does not involve true color vision. Due to the biophysical limitations of visual pigments, spectral sensitivities of photoreceptors are primarily determined by the amino acid sequence structure of expressed opsins, a family of G-protein-coupled receptors (Bowmaker, 1999). The orders of branchiopods studied here, Anotostracans, and Notostracans, have been found to express four and five rhabdomeric opsins in their compound eyes, respectively (Henze & Oakley, 2015; Kashiyama et al., 2009). It was previously unknown how these opsins might contribute to wavelength-dependence of behavioral responses these organisms display. In this study, I place behavioral responses (Chapter 1) in the context of visual physiology by using electroretinography, visual modeling, and phylogenetic comparisons to infer the number of opsin-based classes maintained by the branchiopods studied here. Given the results in the previous chapters, I predicted that these branchiopods use multiple spectral classes, summed for unconventional vision to guide behavioral responses.

Methods

Electrophysiology

Animals reared in Arizona were shipped to the University of Delaware (Lewes, DE), for experiments run during two visits: April 14-22 2013, and August 10-17 2014. Animals were kept in wading pools and exposed to an ambient light cycle immediately following arrival. Extracellular electroretinograms (ERGs) were recorded within one week of arrival and procedures followed those described in (Cohen et al., 2010; Cohen & Frank, 2006). In brief, shrimp were attached to the plastic head of a pin with

cyanoacrylate gel glue, and mounted on an acrylic support within a bath of deionized water. The level of the bath was set to ensure both compound eyes were maintained above water level while the gill-legs were underwater and allowed to beat freely. A metal electrode (100 µm shank width, FHC Inc; Bowdoin, ME) was inserted into the compound eye and served as the recording electrode. Another electrode was placed under the cuticle along the dorsal side of the head to serve as a differential reference. A.C. signals were amplified (Xcell3, FHC Inc; Bowdoin, ME), and stored in LabView (Version 6.1, National Instruments).

A regulated 100 W quartz halogen lamp attached to a monochromator (CM110, Spectral Products; Putnam, CT) was used to provide monochromatic light stimuli. The spectral quality at test wavelengths was further narrowed by blocking filters to ~9nm at full-width half maximum, verified using a spectoradiometer (USB 4000, Ocean Optics; Dunedin, FL). Stimulus irradiance was controlled using a neutral-density wheel (Melles Griot; Rochester, NY) driven by a stepper motor controlled in LabView. Individual flash length was determined using an electromagnetic shutter (Uniblitz, VS25; Rochester, NY). A bifurcated, randomized fiber optic light guide (EXFO; Chelmsford, MA) was used to direct diffuse light centered on a single compound eye, kept at a distance of 1.0 cm. A tungsten filament fiber optic light source (DC-950, Dolan Jenner; Boxborough, MA) with a red bandpass filter (RG630, Schott; Elmsford, NY) was attached to the remaining branch of the fiber optic light guide to provide dim red light for specimen preparation before dark-acclimation. Irradiance was measured at 10-nm intervals using a calibrated radiometric probe and optometer (model S471 optometer, model 260 sensor head, UDT Istruments; San Diego, CA).

After the recording and differential electrodes were set in place, animals were tested periodically with a dim test flash until a consistent dark-acclimated response was maintained for 1 h, indicating the shrimp was dark-acclimated. At this point dark-acclimated spectral sensitivity experiments began. Flashes of 50 ms were used to determine spectral sensitivity at each wavelength (350–690 nm, 20nm intervals), adjusting irradiance to reach a criterion response (0.050 mV) in the peak-to-peak ERG, approximately 0.020 mV above background noise. Test flashes were given between each wavelength to confirm the eye remained dark acclimated. If responses to the test flash changed in a given preparation, data from the animal were not used in subsequent analyses.

Visual modeling of photoreceptor absorptance

I model the absorbance of the fused photoreceptor array per unit length l_j as

$$\xi_j(\lambda) = \sum \alpha_i(\lambda) \frac{A_i}{A} k, \qquad (3a)$$

where α_i is the normalized absorption spectrum of a rhodopsin visual pigment, *Ai/A* is the relative area in cross section of the photoreceptor, and *k* is the peak absorption coefficient. I then calculated the absorptance of the three dimensional tiered photoreceptor array, composed of *j* tiers, as follows,

$$S(\lambda) = \sum \left(Ft_{(j-1)} \left(1 - e^{-\xi_j(\lambda) l_j} \right) \right) \qquad (3b)$$

Where Ft_{j-1} is the fraction of light transmitted by all preceding vertical tiers (1.0 for the first tier). Visual pigment absorption spectra α_i are primarily determined by λ_{max} (Bowmaker, 1999). I used templates developed by (Stavenga, Smits, & Hoenders, 1993),

referred to as SSH from here on, and by (Govardovskii, Fyhrquist, Reuter, Kuzmin, & Donner, 2000), referred to as GFKRD from here on. Both alpha and beta bands were assessed in a preliminary analysis of the global model then only alpha bands were considered. $S(\lambda)$ was normalized to 1 as in (Stavenga & Arikawa, 2011). To infer how many spectral photoreceptor classes branchiopods possess, I used an information criterion approach to select among optimized models of photoreceptor spectral absorptance, given extracellular ERG recordings (Figure 6A,B) and photoreceptor lengths (Chapter 2) measured from dark-acclimated compound eyes. I modeled absorptance of tiered and fused photoreceptor cells for both Notostracans and Anostracans according to Equations 3a and 3b, with all considered models detailed in Appendix D. Parameter estimates, maximum likelihood estimation, and AIC_c calculations follow methods and techniques which are further explained in Chapter 4.

Dark-acclimated spectral sensitivities are most likely to indicate a photoreceptor subset, as metarhodopsin is unlikely to contribute to confounding shifts in spectral sensitivity (Stavenga, 2010). Furthermore, using published data of extracellular recordings from dark-acclimated animals (Chapter 4), this modeling approach correctly identifies four photoreceptor classes which had previously been identified for *Daphnia magna* by chromatic adaptation (K. C. Smith & Macagno, 1990). Branchiopod ommatidia often consist of 6 photoreceptor cells in Anostracans (Elofsson & Odselius, 1975) and 8 in Notostracans (Diersch et al., 1999). Branchiopod ommatidia are fundamentally similar to those of many insects and decapod crustaceans (Melzer, Diersch, Nicastro, & Smola, 1997), which typically have eight photoreceptor cells (R1-R8) with a putative UV or short wavelength-sensitive distal photoreceptor (Kelber &

Henze, 2013; K. C. Smith & Macagno, 1990). I modeled absorptance of tiered and fused photoreceptor cells for both Notostracans and Anostracans according to Equations 3a and 3b, with all considered models detailed in Appendix D.

Opsin alignment and comparison

To identify which opsins correspond to the spectral photoreceptor classes I identified, branchiopod opsin amino acid sequences were first identified from the phylogenies found in (Henze & Oakley, 2015), were downloaded from Genbank (http://www.ncbi.nlm.nih.gov), and aligned in BioEdit v 7.2.5 (Hall, 1999) with a high resolution template sequence of bovine rhodopsin (1U19.pdb) from the Protein Data Bank (http://www.rcsb.org/pdb/; (Berman et al., 2000), and were compared at every site identified as functionally important by (Porter, Cronin, McClellan, & Crandall, 2007).

Results

Spectral Sensitivity

The spectral sensitivity of dark-acclimated *T. longicaudatus* (Figure 6A), and *S. mackini* (Figure 6B) peaked at 510 and 550nm, respectively. The full width half-maximum (FWHM) of the spectral sensitivity function of *T. longicaudatus* extended from 350-650nm, from 350-630nm for *S. mackini* males, and from 470-630nm for *S. mackini* females (Figure 6A and 6B). I did not observe wavelength-specific changes in response waveforms for either species under dark acclimation, with the typical response waveform shown as insets of Figures 6A and 6B.

Photoreceptor absorptance modeling

The comparison between electrophysiology and absorptance modeling shown in Figure 6C-E has identified that both *T. longicaudatus* and *S. mackini* possess four spectral photoreceptor classes (Table 2). As shown by the evidence ratios in this table, model selection was typically unambiguous (all competing models <2.0), indicating the best models have much more support than all other models considered. Our results for male *S. mackini* indicate that modeled peak sensitivities of photoreceptor class λ_{max3} (528nm, Table 2, Figure 6D) closely matches the narrow-bandwidth wavelength-specific behavior I have described at 532nm (Chapter 1).

Evolution of functional variability in opsin binding sites underlying multiple spectral classes

Because amino-acid opsin sequence structure in large part determines the spectral sensitivity of photoreceptors, I compared my modeling results to the most recent rhabdomeric opsin phylogeny of Pancrustacean compound eyes reconciled on a species tree (Figure 7). I aligned opsin sequences to bovine rhodopsin to check amino acid sequence sites which have been found to functionally determine spectral sensitivity. Both Notostraca and Anostraca share a single expressed SW opsin with all Pancrustaceans (Figure 7), that corresponds to spectral photoreceptor λ_{max1} (Table 2). Anostracan and Notostracan MW opsins diversified and were lost within two sub-clades following the divergence of these taxa, (MW1 and MW2, Figure 7). The models shown here provided weak support for five spectral photoreceptor classes in Notostracans (<0.01 $w\text{AIC}_c$, Table 2, Appendix D). The most recently duplicated Notostracan opsin (MW1.b, Figure 7) has

a conserved amino acid binding site which is functionally important for protein compressibility within 4Å when aligned to bovine rhodopsin position 265. In contrast, this amino acid binding site is variable for the most recently duplicated Anostracan opsin (MW2).

Discussion

The multi-model selection procedure has identified that both *T. longicaudatus* and *S. mackini* most likely possess four spectral photoreceptor classes (Table 2). This is consistent with other branchiopods studied to date, as *Daphnia magna* has four spectral classes of photoreceptors with sensitivities spanning 348nm to 608nm (K. C. Smith & Macagno, 1990). Given that all branchiopods are passive dispersers, and are often found in hydrologically isolated, regionally variable freshwater habitats, (Brendonck et al., 2008; Williams, 2005), this suggests that four spectral classes could be maintained for light detection in variable light environments. Most animals that possess four or more spectral photoreceptors have visual demands imposed by their behavior or ecology requiring fine-scale spectral discrimination with corresponding neural processing (Marshall & Arikawa, 2014). For branchiopod crustaceans, I suggest that four spectral photoreceptor classes are instead mainly used for behavior that requires light detection in dim, spectrally variable environments (Figure 1A,B), rather than for object or mate recognition (Nilsson, 2009, 2013).

My results for male *S. mackini* indicate that modeled peak sensitivities of photoreceptor class λ_{max3} (528nm, Table 2, Figure 6D) could be used for the wavelength-specific behavior I have described at 532nm (Chapter 1) to maintain position above

females in the water column. Crustaceans and insects that employ wavelength-specific behavior have been shown to use a subset of their photoreceptors for luminance-driven behavior (Cohen et al., 2010; Kolb & Scherer, 1982). Further, Anostracans have been found to possess a bi-stratified lamina, which anatomically separates photoreceptor terminals into circuits (Nässel et al., 1978). Clearly, future work involving targeted labeling is needed to clarify the neural circuitry of spectral discrimination in branchiopod crustaceans. Synapsin-ir labeling, which has verified that the medulla has been lost in *D. magna,* (Kress et al., 2015) would clarify whether the bi-stratified lamina of Anostracans is the result of a fusion between the proximal lamina and vestiges of a distal medulla. Nevertheless, the modeling I present here suggests that even at the level of the lamina the anatomical separation of neural circuitry is present which could wire a circuit involving a single type of behavior, moving towards light, to λmax_3. These results support the description of this behavior as wavelength-specific, and I predict that similar responses could be found in crustaceans which are likely to use luminance vision to position themselves in the water column.

Evolutionary diversification and convergence of multiple spectral photoreceptor classes:

The genome of *Daphnia pulex* contains the most duplicated opsins of any animal known to date (Colbourne et al., 2011), and the specific opsins that are expressed in branchiopod compound eyes are known for Notostracans and Anostracans (Kashiyama et al., 2009). Spectral classes of photoreceptors are primarily determined by opsin protein sequence (Bowmaker, 1999), and the chromophore is retinal in branchiopods (Kashiyama et al., 2009; K. C. Smith & Macagno, 1990), allowing us to compare my modeling results

to the most recent rhabdomeric opsin phylogeny of Pancrustacean compound eyes (Figure 7) (Henze & Oakley, 2015). Branchiopods express two main Pancrustacean opsin clades, SW and MW, named for sensitivities of the visual pigments inferred by opsin sequence in comparison to well-studied visual systems (Porter et al., 2007). Both Notostraca and Anostraca share a single expressed SW opsin with all Pancrustaceans (Salcedo, Zheng, Phistry, Bagg, & Britt, 2003), that corresponds to spectral photoreceptor λ_{max1} (Table 2). Anostracan and Notostracan MW opsins diversified and were lost within two sub-clades following the divergence of these taxa, suggesting that two of the remaining three spectral classes I have identified most likely converged to similar spectral sensitivities (MW1 and MW2, Figure 7).

Determining the specific opsin identities of these photoreceptor classes will require imaging with *in situ* hybridization. Notostracans have so far been found to express five rhabdomeric opsins, and Anostracans express four (Kashiyama et al., 2009). The models presented here provided low support for five spectral photoreceptor classes in Notostracans (<0.01 $wAIC_c$, Appendix D). The most recently duplicated Notostracan opsin (MW1.b, Figure 7) has a conserved amino acid binding site which has been shown to be functionally important for compressibility within 4Å of bovine rhodopsin position 265 (Porter et al., 2007). These two opsins could potentially be co-expressed in the same photoreceptor. In contrast, this amino acid binding site is variable for the most recently duplicated Anostracan opsin (MW2), supporting four spectral photoreceptor classes. I suggest that a selective history in spectrally variable shallow waters maintains the expression of at least four spectral classes of opsins, as it does in shallow water fishes (Hofmann et al., 2009). Shallow water fishes use four spectral channels for true color

vision (Sabbah, Troje, Gray, & Hawryshyn, 2013), but their environments also do not attenuate light as quickly with depth (Sabbah et al., 2011) as those in which branchiopods are often found. The ancestors of both Pancrustaceans (Henze & Oakley, 2015) and vertebrates (Collin, Davies, Hart, & Hunt, 2009) are thought to have expressed at least four spectral opsin classes, and the present data confirm four spectral classes in branchiopods. Future work is needed to determine if other groups of extant Pancrustaceans which live in variable shallow water environments maintain expression of four spectral classes of photoreceptors. From this study, I conclude that to fully understand the selective pressures which maintain multiple spectral photoreceptor classes, cases in which an animal possesses more spectral photoreceptor classes than would seem warranted by their behavioral repertoire should be considered in addition to true color vision in vision research.

Table 2. Absorptance Model Comparisons for *T. longicaudatus* and *S. mackini*, using Maximum Likelihood and Akaike's Information Criterion Corrected for Small Sample Sizes (AICc). Tiered photoreceptor arrays were modeled for each species and sex using parameters from Equations 3a and 3b. A_i/A, relative area of photoreceptor in cross-section. SSH, rhodopsin visual pigment template (Stavenga et al., 1993). GFRKD, rhodopsin visual pigment template (Govardovskii et al., 2000). Three best supported models (>0.01 $wAIC_c$) are displayed here for each species and sex. All model comparisons considered are included in Appendix D. Evidence ratios were calculated relative to the best model for each species and sex. Models with ambiguous $wAIC_c$ (evidence ratio < 2.0) are indicated by ([a]). Models with low support relative to the best model (evidence ratio > 2.0) are indicated by ([b]).

Species/Sex	Model	λmax_1 (A_1/A)	λmax_2 (A_2/A)	λmax_3 (A_3/A)	λmax_4 (A_4/A)	AIC_c	ΔAIC_c	$wAIC_c$	Evidence Ratio
T. longicaudatus	4,SSH	362 (0.16)	415 (0.34)	500 (0.26)	606 (0.25)	30.4	0	0.470	-
	4,GFKRD[a]	365 (0.15)	414 (0.35)	498 (0.26)	606 (0.24)	30.2	0.184	0.429	1.10
	3,SSH[b]	392 (0.27)	490 (0.49)	602 (0.23)	-	26.9	3.51	0.081	5.78
S. mackini ♂	4,SSH	354 (0.31)	431 (0.16)	528 (0.21)	586 (0.33)	43.7	0	0.881	-
	4,GFKRD[b]	357 (0.30)	429 (0.18)	531 (0.23)	585 (0.29)	39.7	4.00	0.119	7.40
	3,SSH[b]	363 (0.28)	447 (0.15)	560 (0.56)	-	26.8	16.89	<0.01	4666
S. mackini ♀	4,SSH	358 (0.08)	427 (0.14)	541 (0.53)	601 (0.26)	52.0	0	0.548	-
	4,GFKRD[a]	362 (0.08)	428 (0.16)	540 (0.51)	600 (0.25)	51.6	0.39	0.451	1.22
	3,SSH[b]	396 (0.13)	538 (0.58)	597 (0.29)	-	38.8	13.2	<0.01	737

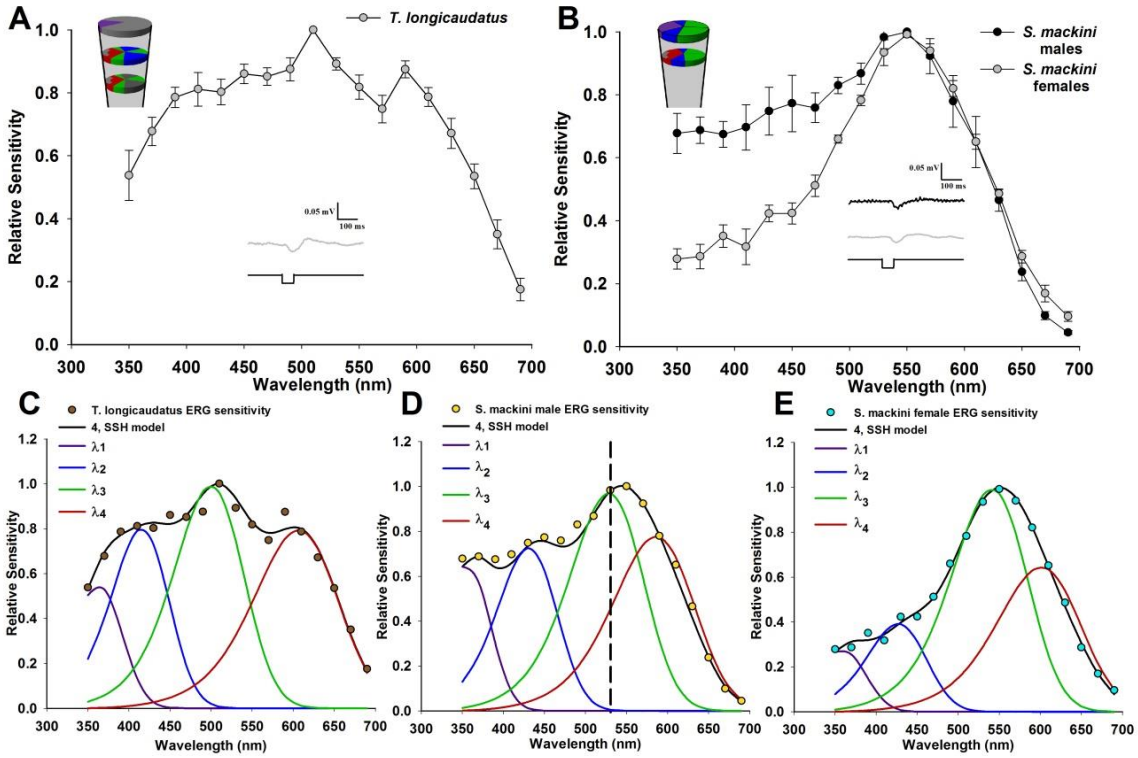

Figure 6. Spectral ERG Sensitivity of Dark-acclimated Branchiopods and Photoreceptor Absorptance Models fit to Branchiopod Spectral ERG Data.
(A and B) ERG data +/- SEM. Representative ERG traces are shown as lower insets with the negative square wave indicating stimulus duration. Upper left insets display ommatidial tiered receptor cell structure (three tiers for *T. longicaudatus*, two tiers for *S.mackini*). The colors represent wavelengths of peak absorptance of best-supported absorptance models for receptor cells or cell-pairs composing spectral channels, with more detail on the specific cell identities in the electronic supplementary material. Modeled relative spectral photoreceptor areas were averaged for male and female *S. mackini*. Grayscale areas in cross-section indicate portions of the rhabdom that do not have microvillar structure (melanin screening pigment or receptor axons) (A) *T. longicaudatus* (n=5). (B) *S. mackini* males and females (n=4). (C-E) ERG data are represented as circles with the best-supported absorptance model curves, 4 SSH rhodopsin visual pigment template for both species (Table 2). Modeled photoreceptor absorptances are included as separate curves with colors representing wavelength of peak absorptance (λ_{max}, Table 2). (C) *T. longicaudatus* (D) *S. mackini* males. The vertical dashed line indicates the wavelength at which behavioral assays found positive movement **towards** the light source (Figure 3C). (E) *S. mackini* females.

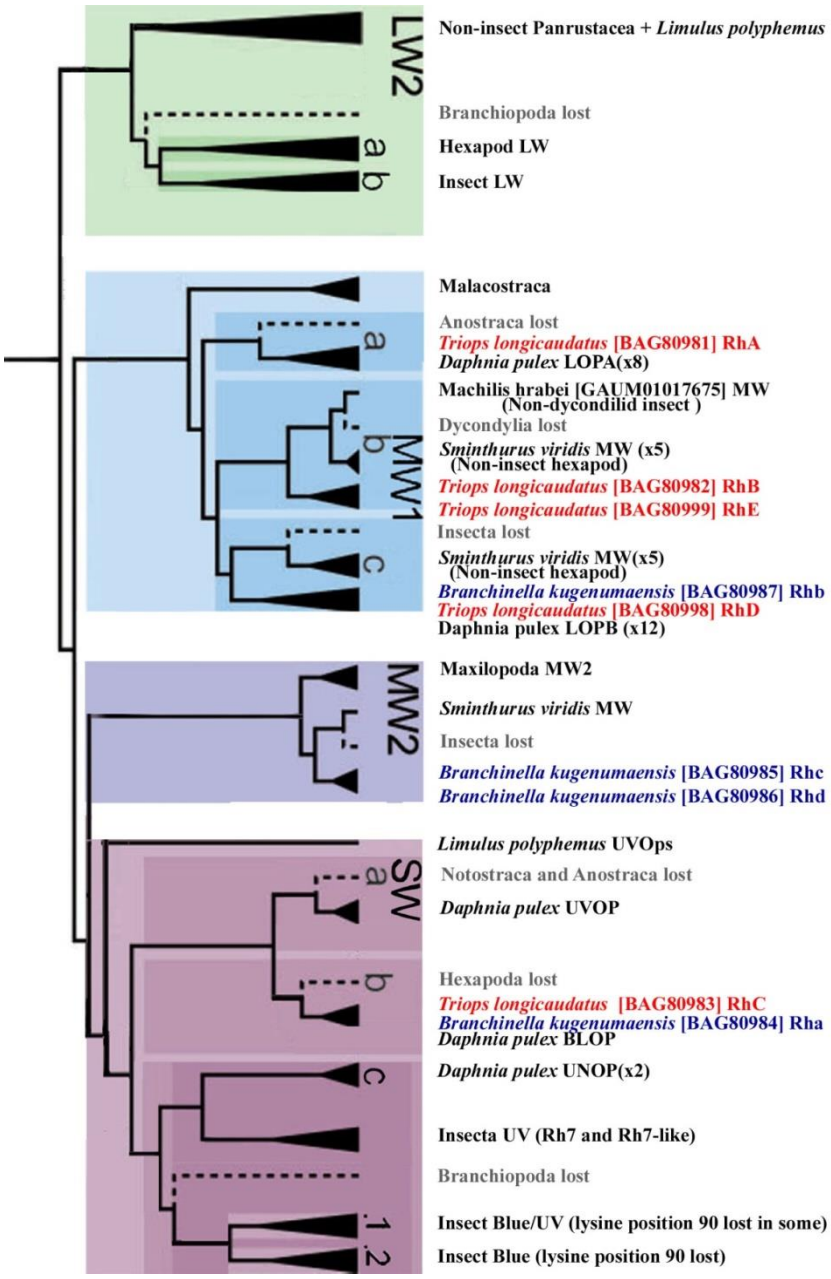

Figure 7. Pancrustacean Rhabdomeric Opsin Phylogeny Reconciled on a Species Tree. After (Henze & Oakley, 2015). Major opsin clades were named by (Henze & Oakley, 2015) for consistency with (Porter et al., 2007), not for known peak spectral sensitivity, and are shaded in green, blue, and purple for long (LW), middle (MW) and short (SW) wavelength clades. Triops longicaudatus (Notostraca) opsins are labeled in red font, and those of Branchinella kugenamensis (Anostraca) are labeled in dark blue font. Dashed lines indicate an inferred loss of an opsin class, labeled gray. Pancrustacean species and opsins which were not informative for branchiopod opsins in the context of Pancrustacea have been pruned from the original figure without changing nodes. Note: Anostraca are not known to express LW clade opsins, as has been corrected in an erratum supplement for Figure 2 in (Henze & Oakley, 2015).

CHAPTER 4

MODELING VISUAL SYSTEM SPECTRAL SENSITIVITIES OF BRANCHIOPODS AND OTHER ORGANISMS

Introduction

Animals possess a diversity of photoreceptor types (Porter et al., 2011), and with the advent of genomic and transcriptomic methods it is now possible to more rigorously identify the functional sites of opsin proteins that determine their spectral sensitivity (Arendt, Tessmar-Raible, Snyman, Dorresteijn, & Wittbrodt, 2004; Porter et al., 2007). The number and wavelength sensitivity of spectral photoreceptor classes which an organism possesses is needed to understand whether the organism can discriminate natural spectra (i.e has some form of color vision), and also to understand the mechanistic context of visually-guided behavior (Kelber & Osorio, 2010).

Spectral classes of photoreceptors are generally identified using a combination of extracellular and intracellular recording techniques (Arikawa, Inokuma, & Eguchi, 1987). Extracellular recordings detect a summed contribution of multiple classes of photoreceptors, including relatively rare classes. It is possible to isolate spectral classes of photoreceptor using chromatic adaptation, where light of a restricted waveband is used to light-adapt single photoreceptor classes. This technique leads to a decrease in sensitivity in the tested waveband. However, because visual pigments are all natively sensitive to short wavelengths (Bowmaker, 1999), the technique is generally only feasible for long wavelength receptors, and for organisms that possess three spectral photoreceptor classes or less (Goldsmith, 1986). Intracellular techniques are most accurate for verifying the

existence of spectral classes, but are time consuming and can be guided by modeling approaches which incorporate physical parameters that can be obtained from histological techniques (Stavenga & Arikawa, 2011).

Here, I describe a method using Akaike's information Criterion to infer, from the spectral sensitivities of the visual systems of four different organisms, the number and relative contributions of spectral photoreceptor classes. This method allows objective comparisons of spectral sensitivity data using examples from published sources to hypotheses of the number and relative contribution of spectral photoreceptor classes in the visual systems of these organisms.

The absorption of multiple classes of photoreceptors in a single optical unit, known as a fused receptor, has been modeled successfully (Snyder, Menzel, & Laughlin, 1973), and I develop these models further to incorporate tiers of receptors. Unfortunately, traditional parametric statistics do not provide a useful framework from which multi-model selection can be used to compare among alternative hypotheses (Burnham & Anderson, 2002). Other researchers have used multi-model selection successfully for oceanic fish to identify the spectral absorbance (equation 4) of different photoreceptor classes (Horodysky, Brill, Warrant, Musick, & Latour, 2008, 2010), but this approach has not yet been used to incorporate knowledge of the physical parameters of the photoreceptor array to model absorptance (equation 5).

Methods

Example selection

The following four organisms were used to examine the abilities and limitations of the described technique.

1) The onycophoran velvet worm, *Principapillatus hitoyensis* (Figure 8A), was used because it expresses only a single spectral opsin class in its photoreceptors (Beckmann et al., 2015).
2) Humans, *Homo sapiens*, possesses three cone (S, M, L) and one rod photoreceptor class (Bradbury & Vehrencamp, 1998). In this study, I use normal human scotopic sensitivity (Figure 8B), represented by S-class cone and rod photoreceptor sensitivities (Bowmaker & Dartnall, 1980; Wyszecki & Stiles, 2000). I also use the scotopic sensitivity of patients with enhanced S-cone syndrome (Figure 8C), a rare condition in which S-cones frequency is increased due to mutations in a transcription factor which controls photoreceptor expression (Haider et al., 2000).
3) The branchiopod crustacean water flea, *Daphnia magna* (Figure 8D), was used because it possesses four spectral classes of photoreceptor (K. C. Smith & Macagno, 1990).
4) The swallow-tail butterfly, *Papilio xuthus* (Figure 8E, F), was used because it possesses at least five main spectral classes of photoreceptor type (Arikawa et al., 1987) in several classes of ommatidia with specialized filtering pigments (Stavenga & Arikawa, 2011).

Data Extraction and binning

Published spectral sensitivity data were digitally extracted using GetData v.2.26 (Fedorov) from (Arikawa et al., 1987; Beckmann et al., 2015; Jacobson, Marmor, Kemp, & Knighton, 1990; K. C. Smith & Macagno, 1990). Where needed, units were converted from log sensitivity to relative sensitivity. Preliminary analysis indicated that 20nm and 10nm wavelength intervals provided identical results. Binning was therefore carried out to 20nm intervals for all sensitivity data extracted. The sensitivity ranges extracted were from 350-690nm, and also from 310-350nm for *D. magna* and *P. xuthus*.

Visual modeling of photoreceptor absorptance

I modeled the absorbance of the fused photoreceptor array per unit length l_j. These equations presented below are identical to those presented in Chapter 3, with the exception that *Ai/A* now represents the relative area *or frequency* in cross section of the photoreceptor,

$$\xi_j(\lambda) = \sum \alpha_i(\lambda) \frac{A_i}{A} k, \qquad \textbf{[4]}$$

where α_i is the normalized absorption spectrum of a rhodopsin visual pigment, *k* is the peak absorption coefficient. Values used for *k* for the invertebrates ($0.008\mu m^{-1}$) were established by (Bruno et al., 1977) and are typical for other crustaceans and insects (Cronin et al., 2014b). Values used for *k* for humans ($0.015\mu m^{-1}$) are typical for vertebrates (Wyszecki & Stiles, 1982). I calculated the absorptance of the three dimensional tiered photoreceptor array, composed of *j* tiers, as follows,

$$S(\lambda) = \sum \left(Ft_{(j-1)} \left(1 - e^{-\xi_j(\lambda) l_j} \right) \right) \qquad \textbf{[5]}$$

Where Ft_{j-1} is the fraction of light transmitted by all preceding vertical tiers (1.0 for the first tier). Visual pigment absorption spectra α_i are primarily determined by λ_{max} (Bowmaker, 1999). I use templates developed by (Stavenga et al., 1993 and by (Govardovskii et al., 2000), referred to as SSH and GFKRD, respectively. Both alpha and beta bands were assessed in a preliminary analysis of the global model then only alpha bands were considered. *S(λ)* was normalized to 1 as in (Stavenga & Arikawa, 2011).

Incorporating known photoreceptor lengths, l_j, from equation 5

The following photoreceptor lengths were estimated or taken from published sources for each organism. *P. hitoyensis* (100μm) (Beckmann et al., 2015); *H. sapiens* (22.5 μm) (Cronin et al., 2014a); *Daphnia magna* (12.0 μm) (K. C. Smith & Macagno, 1990); *Papilio xuthus* (500 μm) (Arikawa & Stavenga, 1997). Further, how specific photoreceptors contribute to a fused cross-section, and tiered three-dimensional photoreceptor array is known for *D. magna* and for *P. xuthus*. As in many insects and crustaceans (Kelber & Henze, 2013), for both species the shortest wavelength receptor becomes axon-like partway through the optical unit and all models used here with more than one spectral class of photoreceptor incorporate this structure. For *D. magna*, the shortest wavelength receptor forms a fused structure in the distal (upper) half of the optical unit (6.0 μm), with a short-wavelength receptors replaced by a long-wavelength sensitive receptor in the proximal (lower) half of the optical unit (6.0um). For *P. xuthus*, the distal two-thirds of the optical unit (333 μm) are modeled as a single optical unit, replaced by a long wavelength receptor in the proximal portion (167 μm)

Parameter estimates, maximum likelihood estimation, optimization, and AIC_c procedure:

The maximum likelihood estimate (MLE) was calculated according to (Burnham & Anderson, 2002)

$$\log(L(\underline{\hat{\theta}}) = -\frac{1}{2}\log(\hat{\sigma}^2) - \frac{n}{2}\log(2\pi) - \frac{n}{2}, \qquad \textbf{[5]}$$

where the ML estimator for $\hat{\sigma}^2$ is $\frac{RSS}{n}$, and RSS is the residual sum of squares for a given model. Optimization of model parameters (λ_{max}, and A*i*/A) was carried out using custom MATLAB scripts, and the Optimization Toolbox.

I used Akaike's information criterion for small samples (AIC_c) to compare the optimized log-likelihood,

$$AIC_c = -2\log(L(\underline{\hat{\theta}}) + \frac{2K(K+1)}{n-K-1}, \qquad \textbf{[6]}$$

where *K* is the number of parameters for a given model. AIC scores were all weighted in relation to the best model to calculate evidence ratios shown in Tables 3 and 4 and Appendices E and F (Burnham & Anderson, 2002). AIC is an objective measure that imposes a realistic penalty for over-parameterization (Burnham & Anderson, 2002). AIC scores were first compared to the best model ($\Delta AIC_c = AIC - minAIC$), then were compared using Akaike weights,

$$wAIC_C = \frac{e^{-0.5\Delta AIC_i}}{\sum_1^R e^{-0.5\Delta AIC_r}}, \qquad \textbf{[7]}$$

Where *R* is the number of models considered. Effectively, $wAIC_C$ provides a weighting which indicates the likelihood of a single optimized model in context of all models which were considered, given the penalty for over-parameterization. I then use Akaike weights

to calculate evidence ratios relative to the best model shown in Tables 3 and 4. AIC is an objective measure that imposes a realistic penalty for over-parameterization (Burnham & Anderson, 2002).

I first used this procedure to optimize models to extracellular data for *D. magna* in which beta bands were considered at every possible photoreceptor, an "all subsets" regression examining the influence of each parameter on correct model selection. The regression results indicated that beta bands were uninformative for model selection as they were the least important variables and upon removal led to a reduction in AIC_c according to methods outlined in (Arnold, 2010; Burnham & Anderson, 2002). Beta bands at each photoreceptor position were therefore removed as a parameter and only the models in Appendices D-F were included for the formal analyses.

Results

AIC_c results presented in Tables 3 and 4 indicate the most likely models, given the data I have extracted for these organisms. The first row for each organism indicates the parameters which were found empirically from the cited sources. As shown by the evidence ratios in these tables, model selection was typically unambiguous (all competing models <2.0), indicating the best models have much more support than all other models considered. For *P. hitoyensis,* the best model indicates a single spectral photoreceptor class (Table 3). For normal humans and enhanced S-cone patients, the best models indicate two spectral photoreceptor classes corresponding to S-cones and rod photoreceptors. This method also finds a higher frequency of λ_{max1} photoreceptors for enhanced S-cone patients than in normal humans (Table 3). For *Daphnia magna,* the best

model indicates four spectral photoreceptors, including a UV receptor (Table 4). The second best model for *D. magna* was a three receptor SSH template absorptance model, indicating it was more likely than the optimized four receptor GFKRD absorptance model. For *Papilio xuthus,* absorptance models do not correspond to the five main photoreceptor classes which are known (Table 4), as the technique selects a two receptor array. Absorbance models do support five photoreceptor classes (Table 4).

Discussion

With the exception of *Papilio xuthus* absorptance model selection, this technique converges on the same answers provided in the literature. As can be seen from the fit of each best model to the data (Figure 8), and from the evidence ratios (Tables 3 and 4), the technique described here is generally able to resolve the number and relative cross sectional area or frequency of the photoreceptors in the visual systems I have modeled. I will discuss the results from each species separately.

1) Velvet worm *P. hitoyensis* sensitivity (Figure 8A) is known to be represented by a single spectral opsin class expressed in its photoreceptors (Beckmann et al., 2015). Though one to five spectral classes were considered (Table 3 and Appendix E), this example clearly illustrates the penalty imposed for additional parameters by AIC. In order to add parameters (i.e. more complex models), the likelihood of those models, given the data, must outweigh the penalty imposed by additional parameters. In this example, all optimized models with additional photoreceptors did not improve the likelihood estimate (MLE) sufficiently for any

of them to be selected, leading to realistic model selection of a single photoreceptor class.

2) Normal and Enhanced S cone Human scotopic sensitivities (Figure 8B and 8C) is known for normal humans to be represented by S-class cone and rod photoreceptor sensitivities, and with a higher frequency of S cones in patients that have Enhanced S Cone syndrome (Haider et al., 2000; Hood, Cideciyan, Roman, & Jacobson, 1995; Jacobson et al., 1990). Human absorptance models are corrected for transmittance through the lens and a distal macula layer which protects the retina, but which does not contribute to spectral sensitivity (Figure 8B and 8C gray lines) (Wyszecki & Stiles, 2000). This example illustrates that if an absorptive layer exists which does not contribute to spectral sensitivity, a relatively narrow spectral sensitivity such as that of dark-acclimated humans can underlie two or more spectral classes of photoreceptors. This is important to bear in mind, because if such absorptive layers are overlooked, model selection will be poor. Alternatively, poor model selection can also notify a researcher that such a layer exists and should be verified empirically.

3) *Daphnia magna* sensitivity (Figure 8C) is known to be represented by four spectral photoreceptor classes with a distal UV receptor (K. C. Smith & Macagno, 1990). *D. magna* data were best supported by a four receptor SSH absorptance model, and the second best model was a three receptor SSH model, rather than a four receptor GFKRD model. This finding can be explained by worse performance of the GFKRD template than the SSH template in the UV range (Stavenga, 2010), and indicates that future modeling efforts for organisms that

have sensitivity in the UV range should expect better cumulative performance of photoreceptor arrays which are based on the SSH template. It should also be noted that the relative cross section (A_i/A) of each photoreceptor class may not match the relative sensitivity at its peak wavelength (for example A_2,A_3) and the reason for this is that if these photoreceptors are known to contribute along the entire vertical length of the optical unit, the cross-sectional area of the optimized models at a given section would be less than the contribution of those receptors along an entire three-dimensional unit.

4) *Papilio xuthus* sensitivity (Figure 8E and F), averaged from extracellular recordings from multiple positions in the compound eye, is known to be represented by five main spectral photoreceptor classes (Arikawa et al., 1987). Roughly two-dimensional absorbance (Figure 8F given by eq. 3A) at a cross-section two thirds from the distal tip of the rhabdom of an ommatidium selects 5 spectral photoreceptor classes, with the largest deviations of each spectral class known to contain specialized filters (Wakakuwa et al., 2007). Absorptance models (Figure 8E, dashed lines) illustrate poor results with this technique for *Papilio xuthus* because of model-oversimplification: as can be seen by the very broad (>100 μm) sensitivity of each modeled photoreceptor in the "best" model, self-screening has been over-estimated, and in fact *Papilio xuthus* is known to employ several specialized filtering pigments heterogeneously in ommatidia of different regions of their compound eyes, in part to avoid this effect (Arikawa & Stavenga, 1997). The factors that were over-simplified by the models used here are further explained in context of the overall technique below.

Although the inferences from this multi-model selection technique match the empirical evidence well, the technique must still be employed judiciously taking ito consideration what is known of the structural features of a given visual system. *Papilio xuthus* is a case in point; five main spectral photoreceptor classes are found in cross-section approximately two-thirds of the way through their ommatidia, and absorbance results presented here support this finding because of the following details that were not captured by the models used here: *P. xuthus* compound eyes are composed of multiple classes of ommatidia, which compose regions of differing spectral sensitivity (Arikawa et al., 1987; Arikawa, 2003). To add to this interesting complexity, some of the spectral classes of receptors supported by the absorbance results of this technique (λmax_1, λmax_2 and λmax_5, Table 4), have filtering pigments in similar spectral regions which serve to sharpen spectral sensitivity, but also lead to the largest deviations in λmax from known intracellular work, in comparison to the accurate values of λmax_3 and λmax_4. This further demonstrates that poor model selection indicates the presence of biologically interesting absorptive layering.

Since there is no evidence that branchiopods use specialized filtering pigments(Martin, 1992; K. C. Smith & Macagno, 1990), and our results from Chapter 2 indicate that much spatial resolution is lost for behaviors I have described (Chapter 1), I predict that this type of technique will find most utility for eyes that are optimized for unconventional vision in spectrally variable environments. I suggest that these models should be used in the future, as deviations from these models can identify spectral filtering which was previously unknown for an organism, or can provide validation in the context of what is known of their visual system.

Table 3.

Absorptance Model Comparisons for *P. hitoyensis* and *Homo sapiens* Using Maximum Likelihood and Akaike's Information Criterion Corrected for Small Sample Sizes (AICc). Tiered photoreceptor arrays were modeled for each species and sex using parameters from Equations 4 and 5. A_i/A, relative area of photoreceptor in cross-section, or relative frequency. SSH, rhodopsin visual pigment template (Stavenga et al., 1993). GFRKD, rhodopsin visual pigment template (Govardovskii et al., 2000). Three best supported models (>0.01 $wAIC_c$) are displayed here for each species and condition. All model comparisons considered are included in Appendix E. Evidence ratios were calculated relative to the best model for each species and sex. Models with ambiguous $wAIC_c$ (evidence ratio < 2.0) are indicated by ([a]). Models with low support relative to the best model (evidence ratio > 2.0) are indicated by ([b]).

Species/Condition	(Reference) Model	λmax_1 (A_1/A)	λmax_2 (A_2/A)	λmax_3 (A_3/A)	λmax_4 (A_4/A)	AIC_c	ΔAIC_c	$wAIC_c$	Evidence Ratio
P.hitoyensis	(Beckmann et al., 2015)	484	-	-	-	-	-	-	-
	1,GFKRD	481 (1.0)	-	-	-	55.76	0	0.508	-
	1,SSH[a]	481 (1.0)	-	-	-	54.90	0.863	0.330	1.54
	2, GFKRD[b]	481 (0.70)	481 (0.30)	-	-	53.22	2.54	0.143	3.56
Normal Human (scotopic)	Wyszecki and Stiles, 2000)	420	497	-	-	-	-	-	-
	2,SSH	421 (0.16)	495 (0.85)	-	-	91.31	0	0.500	-
	2,GFKRD[b]	419 (0.1 7)	495 (0.83)	-	-	91.13	0.176	0.458	1.09
	3,SSH[b]	407 (0.11)	493 (0.45)	493 (0.45)	-	85.1	6.24	0.02	22.6
Enchanced S-cone Human (scotopic)		420	497	-	-	-	-	-	-
	2,SSH	429 (0.76)	506 (0.24)	-	-	65.57	0	0.587	-
	2,GFKRD[a]	429 (0.75)	506 (0.25)	-	-	63.96	1.62	0.261	2.25
	3, GFKRD[b]	375 (0.27)	432 (0.54)	507 (0.20)	-	61.79	3.79	0.088	6.65

Table 4. Absorptance Model Comparisons for *Daphnia magna* and *Papilio xuthus* Using Maximum Likelihood and Akaike's Information Criterion Corrected for Small Sample Sizes (AICc)**.** Tiered photoreceptor arrays were modeled for each species and sex using parameters from Equations 4 and 5. A_i/A, relative area of photoreceptor in cross-section, or relative frequency. SSH, rhodopsin visual pigment template (Stavenga et al., 1993). GFRKD, rhodopsin visual pigment template (Govardovskii et al., 2000). Three best supported models (>0.01 $w\text{AIC}_c$) are displayed here for each species and condition. All model comparisons considered are included in Appendix F. Evidence ratios were calculated relative to the best model for each species and sex. Models with ambiguous $w\text{AIC}_c$ (evidence ratio < 2.0) are indicated by ([a]). Models with low support relative to the best model (evidence ratio > 2.0) are indicated by ([b]).

Species/Condition	(Reference) Model	λmax_1 (A_1/A)	λmax_2 (A_2/A)	λmax_3 (A_3/A)	λmax_4 (A_4/A)	λmax_5 (A_5/A)	AIC_c	ΔAIC_c	$wAIC_c$	Evidence Ratio
D. magna (Tiered absorptance)	(K. C. Smith & Macagno, 1990)	348	434	525	608	-	-	-	-	-
	4,SSH	362 (0.52)	415 (0.21)	500 (0.12)	606 (0.15)	-	46.24	0	0.979	-
	3, SSH[b]	367 (0.50)	455 (0.22)	560 (0.28)	-	-	38.28	7.96	0.018	53.64
	4, GFKRD[b]	364 (0.50)	437 (0.21)	508 (0.12)	582 (0.17)	-	33.27	12.97	<0.01	656
P. xuthus (Tiered absorptance)	(Arikawa et al., 1987)	360	390/400	460	520	600	-	-	-	-
	2,SSH	429 (0.48)	529 (0.52)	-	-	-	34.85	0	0.726	-
	3,SSH [b]	429 (0.56)	505 (0.23)	559 (0.21)	-	-	31.38	3.477	0.128	5.69
	2,GFKRD[b]	422 (0.49)	529 (0.51)	-	-	-	30.46	4.389	0.081	8.98
P. xuthus (Absorbance)	(Arikawa et al., 1987)	360	390/400	460	520	600				
	5, GFKRD	346 (0.10)	381 (0.25)	457 (0.32)	529 (0.20)	586 (0.12)	50.38	0	0.653	-
	3, SSH[b]	371 (0.35)	463 (0.37)	557 (0.28)	-		47.76	2.63	0.176	3.71
	4, GFKRD [b]	348 (0.13)	385 (0.26)	465 (0.36)	559 (0.25)		46.56	3.83	0.096	6.77

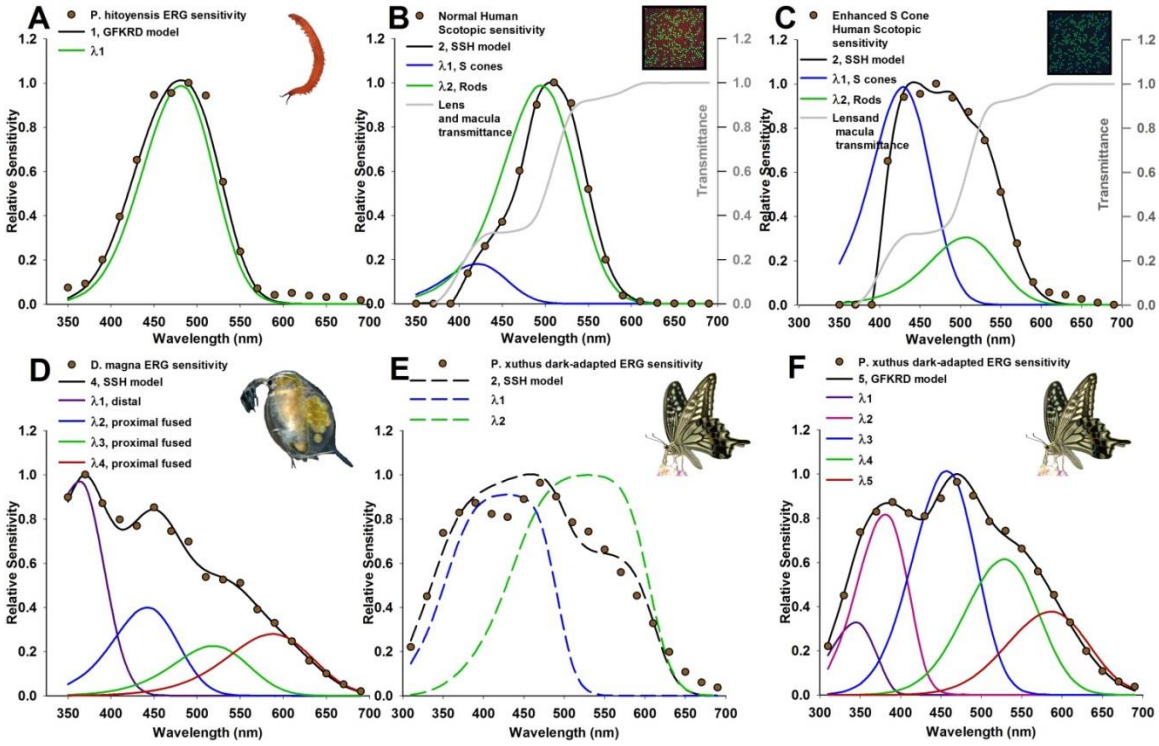

Figure 8. Photoreceptor Absorptance Models Based on Known Photoreceptor Lengths and Vertical Tiering, Fit to Relative Spectral Sensitivity Data Extracted From Published Sources. Models were selected using Akaike's Information Criterion corrected for small sample sizes (AIC_c) with the best three models shown in Tables 3 and 4, and all models in Appendices E and F. Models are represented by curves and extracted data are indicated by data points. (A) Velvet worm *P. hitoyensis* sensitivity. (B and C) Normal and Enhanced S cone Human scotopic sensitivities. D) *Daphnia magna* sensitivity. (E and F) *Papilio xuthus* sensitivity, averaged from extracellular recordings from multiple positions in the compound eye. (E) Absorptance models (dashed lines) (F). Two-dimensional absorbance (given by eq.1) at a cross-section approximately two thirds from the distal tip of the rhabdom of an ommatidium.

CONCLUDING REMARKS

In this dissertation, I addressed the question of why branchiopod crustaceans have multiple opsin-based visual pigments in their visual systems, and whether they have unconventional vision. Before these studies, it was unknown how the multiple-pigment visual systems of Notostracan or Anostracan branchiopods contributed to their visually-guided behavior. Based on the requirements for color vision I have addressed, the expression of multiple opsins in branchiopod visual systems suggested color vision, but the simplified neural systems of branchiopods suggested that they might have reduced color processing ability or unconventional vision, as summarized in Figure i.1.

I first showed that Notostracans and Anostracans use light as a cue to behaviorally regulate their vertical position in the water column. Their behavioral responses to different wavelength stimuli suggested use of multiple photoreceptor classes at dim intensities. I found that the spectral light environment of their habitats in Arizona is variable. I found that ephemeral pools reach low intensities at shallow depth due to rapid attenuation in the water column.

To explore how these animals detect light in such low intensity conditions, I modeled the minimum intensities at which their compound eyes and median eyes can operate, and found that their compound eyes can operate below starlight, if they incorporate neural summation in the lamina of their optic lobe. I took electroretinographic recordings to find the dark-acclimated spectral sensitivities of their compound eyes, and found broad spectral sensitivity. Using models of spectral absorptance, and a multi-model selection approach, I inferred that both Notostracan and Anostracan branchiopods possess four spectral classes of photoreceptors in their

compound eyes. I then extended the modeling approach to three other organisms, and have found that models of spectral absorptance correspond to empirical data of photoreceptor spectral classes. Future studies should incorporate spectral absorptance models to identify whether spectral photoreceptor classes contribute to unconventional vision and behavior.

This work has led me to propose that branchiopods have unconventional vision and sum the responses from multiple spectral classes to maintain vision at depth. By understanding the number of potential spectral classes of photoreceptors an animal possesses and which spectral classes guide their specific behaviors, it becomes possible to identify if they use conventional or unconventional vision (Figure i.1) and to better understand the selective pressures that maintain arrays of multiple classes of spectral photoreceptors, and subsequent processing layers in animal visual systems.

REFERENCES

Arendt, D., Tessmar-Raible, K., Snyman, H., Dorresteijn, A. W., & Wittbrodt, J. (2004). Ciliary Photoreceptors with a Vertebrate-Type Opsin in an Invertebrate Brain. *Science*, *306*(5697), 869–871.

Arikawa, K. (2003). Spectral organization of the eye of a butterfly, Papilio. *Journal of Comparative Physiology A*, *189*(11), 791–800.

Arikawa, K., Inokuma, K., & Eguchi, E. (1987). Pentachromatic visual system in a butterfly. *Naturwissenschaften*, *74*(6), 297–298.

Arikawa, K., & Stavenga, D. G. (1997). Random array of colour filters in the eyes of butterflies. *Journal of Experimental Biology*, *200*(19), 2501–2506.

Arnold, T. W. (2010). Uninformative Parameters and Model Selection Using Akaike's Information Criterion. *The Journal of Wildlife Management*, *74*(6), 1175–1178.

Beckmann, H., Hering, L., Henze, M. J., Kelber, A., Stevenson, P. A., & Mayer, G. (2015). Spectral sensitivity in Onychophora (velvet worms) revealed by electroretinograms, phototactic behaviour and opsin gene expression. *Journal of Experimental Biology*, *218*(6), 915–922.

Belk, D. (1975). Key to the Anostraca (Fairy Shrimps) of North America. *The Southwestern Naturalist*, *20*(1), 91.

Belk, D., & Martin, J. W. (1991). Anostracan Mating Behavior: A Case of Scramble Competition Polygyny. In *Crustacean Sexual Biology* (pp. 111–125).

Berman, H. M., Westbrook, J., Feng, Z., Gilliland, G., Bhat, T. N., Weissig, H., … Bourne, P. E. (2000). The Protein Data Bank. *Nucleic Acids Research*, *28*(1), 235–242.

Bowmaker, J. K. (1999). Molecular biology of photoreceptor spectral sensitivity. In *Adaptive Mechanisms in the Ecology of Vision* (pp. 439–464). Dordrecht: Kluwer Academic Publishers.

Bowmaker, J. K., & Dartnall, H. J. (1980). Visual pigments of rods and cones in a human retina. *The Journal of Physiology*, *298*(1), 501–511.

Bradbury, J., & Vehrencamp, S. (1998). *Principles of Animal Communication*. New York, NY: Sinauer Associates.

Brendonck, L. (1996). Diapause, quiescence, hatching requirements: what we can learn frmo large freshwater branchiopods (Crustacea: Branchiopoda: Anostraca,

Notostraca, Conchostraca). *Hydrobiologia*, *320*, 85–97.

Brendonck, L., Rogers, D. C., Olesen, J., Weeks, S., & Hoeh, W. R. (2008). Global diversity of large branchiopods (Crustacea: Branchiopoda) in freshwater. *Hydrobiologia*, *595*(1), 167–176.

Bruno, M., Barnes, S., & Goldsmith, T. H. (1977). The visual pigment and visual cycle of the lobster,Homarus. *Journal of Comparative Physiology*, *120*(2), 123–142.

Burnham, K. P., & Anderson, D. R. (2002). *Model selection and multimodel inference: a practical information-theoretic approach*. New York, NY: Springer Science & Business Media.

Carleton, K. L., Spady, T. C., & Kocher, T. D. (2006). Visual communication of African cichlid fishes in a phylogenetic context. In F. Ladich, C. SP, M. P, & K. BG (Eds.), *Communication in Fishes* (pp. 487–515). Chicago.

Centeno, M. D., Brendonck, L., & Persoone, G. (1993). Cyst-based toxicity tests. III. Development and standardization of an acute toxicity test with the freshwater anostracan crustacean Streptocephalus proboscideus. In *Progress in standardization of aquatic toxicity tests* (pp. 37–55). Lewis Publishers.

Cohen, J. H., Cronin, T. W., Lessios, N., & Forward, R. B. (2010). Visual physiology underlying orientation and diel behavior in the sand beach amphipod Talorchestia longicornis. *The Journal of Experimental Biology*, *213*(Pt 22), 3843–51.

Cohen, J. H., & Forward, R. B. (2009). Zooplankton Diel Vertical Migration - A Review of Proximate Control. *Oceanography and Marine Biology: An Annual Review*, *47*, 77–110.

Cohen, J. H., & Frank, T. M. (2006). Visual physiology of the Antarctic amphipod Abyssorchomene plebs. *The Biological Bulletin*, *211*(2), 140–8.

Colbourne, J. K., Pfrender, M. E., Gilbert, D., Thomas, W. K., Tucker, A., Oakley, T. H., … Boore, J. L. (2011). The ecoresponsive genome of Daphnia pulex. *Science (New York, N.Y.)*, *331*(6017), 555–61.

Collin, S. P., Davies, W. L., Hart, N. S., & Hunt, D. M. (2009). The evolution of early vertebrate photoreceptors. *Philosophical Transactions of the Royal Society of London B: Biological Sciences*, *364*(1531), 2925–2940.

Consi, T. R., & Macagno, E. R. (1985). The spectral sensitivity of eye movements in response to light flashes in Daphnia magna. *Journal of Comparative Physiology A: Neuroethology, Sensory, Neural, and Behavioral Physiology*, *156*(1), 135–143.

Cronin, T. W. (2005). Invertebrate Vision in Water. In E. J. Warrant & D.-E. Nilsson (Eds.), *Invertebrate Vision* (pp. 211–249). Cambridge Unversity Press.

Cronin, T. W., & Forward, R. B. (1988). The visual pigments of crabs. *Journal of Comparative Physiology A: Neuroethology, Sensory, Neural, and Behavioral Physiology*, *162*(4), 463–478.

Cronin, T. W., Johnsen, S., Marshall, N. J., & Warrant, E. J. (2014a). *Visual ecology*. Princeton University Press.

Cronin, T. W., Johnsen, S., Marshall, N. J., & Warrant, E. J. (2014b). Visual Pigments and Photoreceptors. In *Visual ecology* (pp. 37–65). Princeton University Press.

Cummings, M. E. (2007). Sensory trade-offs predict signal divergence in surfperch. *Evolution*, *61*(3), 530–45.

De Meester, L., Dawidowicz, P., van Gool, E., & Loose, C. (1999). Ecology and evolution of predator-induced behavior of zooplankton: depth selection behavior and diel vertical migration. In R. Tollrian & C. D. Harvell (Eds.), *Ecology and Evolution of Inducible Defenses* (pp. 160–176). Princeton, New Jersey: Princeton University Press.

Diersch, R., Melzer, R. R., & Smola, U. (1999). Morphology of the Compound Eyes of Two Ancestral Phyllopods, Triops cancriformis and Lepidurus apus (Notostraca: Triopsidae). *Journal of Crustacean Biology*, *19*(2), 313–323.

Dumont, H. J., & Negrea, S. V. (2002). *Introduction to the Class Branchiopoda*. Backhuys Publishers.

Dyer, A. G., Paulk, A. C., & Reser, D. H. (2011). Colour processing in complex environments: insights from the visual system of bees. *Proceedings. Biological Sciences / The Royal Society*, *278*(1707), 952–9.

Elofsson, R. (1966). The nauplius eye and frontal organs of the non-Malacostraca (Crustacea). *Sarsia*, *25*(1), 1–128.

Elofsson, R., & Odselius, R. (1975). The Anostracan Rhabdom and the Basement Membrane. An Ultrastructural Study of the Artemia Compound Eye (Crustacea). *Acta Zoologica*, *56*(2), 141–153.

Endler, J. A. (1992). Signals , Signal Conditions , and the Direction of Evolution. *The American Naturalist*, *139*, 125–153.

Folmer, O., Black, M., Hoeh, W., Lutz, R., & Vrijenhoek, R. (1994). DNA primers for amplification of mitochondrial cytochrome c oxidase subunit I from diverse

metazoan invertebrates. *Molecular Marine Biology and Biotechnology*, *3*(5), 294–299.

Forward, R. B., Bourla, M. H., Lessios, N. N., & Cohen, J. H. (2009). Orientation to shorelines by the supratidal amphipod Talorchestia longicornis: Wavelength specific behavior during sun compass orientation. *Journal of Experimental Marine Biology and Ecology*, *376*(2), 102–109.

Forward, R. B., Cronin, T. W., & Douglass, J. K. (1988). The visual pigments of crabs. *Journal of Comparative Physiology A: Neuroethology, Sensory, Neural, and Behavioral Physiology*, *162*(4), 479–490.

Fugate, M. (1992). *Speciation in the fairy shrimp genus Branchinecta (Crustacea: Anostraca) from North America*. *Proquest Dissertations and Theses*.

Gao, S., Takemura, S., Ting, C.-Y., Huang, S., Lu, Z., Luan, H., … Lee, C.-H. (2008). The Neural Substrate of Spectral Preference in Drosophila. *Neuron*, *60*(2), 328–342.

Goldsmith, T. H. (1986). Interpreting trans-retinal recordings of spectral sensitivity. *Journal of Comparative Physiology A*, *159*(4), 481–487.

Goldsmith, T. H. (1990). Optimization, Constraint, and History in the Evolution of Eyes. *The Quarterly Review of Biology*, *65*(3), 281–322.

Govardovskii, V. I., Fyhrquist, N., Reuter, T., Kuzmin, D. G., & Donner, K. (2000). In search of the visual pigment template. *Visual Neuroscience*, *17*(04), 509–528.

Haider, N. B., Jacobson, S. G., Cideciyan, A. V, Swiderski, R., Streb, L. M., Searby, C., … Sheffield, V. C. (2000). Mutation of a nuclear receptor gene, NR2E3, causes enhanced S cone syndrome, a disorder of retinal cell fate. *Nat Genet*, *24*(2), 127–131.

Hall, T. A. (1999). BioEdit: a user-friendly biological sequence alignment editor and analysis program for Windows 95/98/NT. In *Nucleic acids symposium series* (Vol. 41, pp. 95–98).

Henze, M. J., & Oakley, T. H. (2015). The Dynamic Evolutionary History of Pancrustacean Eyes and Opsins. *Integrative and Comparative Biology*, *55*(5), 830–842.

Hochberg, Y. (1988). A sharper Bonferroni procedure for multiple tests of significance. *Biometrika*, *75*(4), 800–802.

Hofmann, C. M., O'Quin, K. E., Marshall, N. J., Cronin, T. W., Seehausen, O., & Carleton, K. L. (2009). The eyes have it: regulatory and structural changes both underlie cichlid visual pigment diversity. *PLoS Biology*, *7*(12), e1000266.

Hood, D. C., Cideciyan, A. V, Roman, A. J., & Jacobson, S. G. (1995). Enhanced S cone syndrome: Evidence for an abnormally large number of S cones. *Vision Research*, *35*(10), 1473–1481.

Horodysky, A. Z., Brill, R. W., Warrant, E. J., Musick, J. A., & Latour, R. J. (2008). Comparative visual function in five sciaenid fishes inhabiting Chesapeake Bay. *Journal of Experimental Biology*, *211*(22), 3601–3612.

Horodysky, A. Z., Brill, R. W., Warrant, E. J., Musick, J. A., & Latour, R. J. (2010). Comparative visual function in four piscivorous fishes inhabiting Chesapeake Bay. *Journal of Experimental Biology*, *213*(10), 1751–1761.

Jacobson, S. G., Marmor, M. F., Kemp, C. M., & Knighton, R. W. (1990). SWS (blue) cone hypersensitivity in a newly identified retinal degeneration. *Investigative Ophthalmology & Visual Science*, *31*(5), 827–838.

Jerlov, N. G. (1968). *Optical oceanography*. New York, NY: Elsevier Science, Inc.

Jerlov, N. G. (1976). *Marine Optics*. Amsterdam: Elsevier.

Kashiyama, K., Seki, T., Numata, H., & Goto, S. G. (2009). Molecular characterization of visual pigments in Branchiopoda and the evolution of opsins in Arthropoda. *Molecular Biology and Evolution*, *26*(2), 299–311.

Kelber, A. (2005). Invertebrate Colour Vision. In E. J. Warrant & D.-E. Nilsson (Eds.), *Invertebrate Vision* (pp. 250–290). Cambridge: Cambridge Unversity Press.

Kelber, A., Balkenius, A., & Warrant, E. J. (2002). Scotopic colour vision in nocturnal hawkmoths. *Nature*, *419*(6910), 922–925.

Kelber, A., & Henze, M. J. (2013). Colour Vision: Parallel Pathways Intersect in Drosophila. *Current Biology*, *23*(23), R1043–R1045.

Kelber, A., & Lind, O. (2010). Limits of colour vision in dim light. *Ophthalmic & Physiological Optics : The Journal of the British College of Ophthalmic Opticians (Optometrists)*, *30*(5), 454–9.

Kelber, A., & Osorio, D. (2010). From spectral information to animal colour vision: experiments and concepts. *Proceedings. Biological Sciences / The Royal Society*, *277*(1688), 1617–25.

Kerfoot, C. W., & Lynch, M. (1987). Branchiopod Communities associations with panktivorous fish in space and time. In *Predation: Direct and indirect impacts on aquatic communities* (pp. 367–378). University Press of New England.

Kleinlogel, S., Marshall, N. J., Horwood, J. M., & Land, M. F. (2003). Neuroarchitecture of the color and polarization vision system of the stomatopod Haptosquilla. *The Journal of Comparative Neurology*, *467*(3), 326–42.

Kolb, G., & Scherer, C. (1982). Experiments on wavelength specific behavior of Pieris brassicae L. During drumming and egg-laying. *Journal of Comparative Physiology. A, Neuroethology, Sensory, Neural, and Behavioral Physiology*, *149*(3), 325–332.

Kress, T., Harzsch, S., & Dircksen, H. (2015). Neuroanatomy of the optic ganglia and central brain of the water flea Daphnia magna (Crustacea, Cladocera). *Cell and Tissue Research*, 1–29.

Land, M. F., & Nilsson, D.-E. (2005). General-purpose and special-purpose visual systems. In E. J. Warrant & D.-E. Nilsson (Eds.), *Invertebrate Vision* (pp. 167–210). Cambridge: Cambridge University Press.

Land, M. F., & Nilsson, D.-E. (2012). *Animal eyes* (2nd ed.). New York, NY: Oxford University Press.

Laughlin, S. B. (1981). Neural principles in the peripheral visual systems of invertebrates. In *Comparative Physiology and Evolution of Vision in Invertebrates: Invertebrate Visual Centers and Behavior I, Handbook of Sensory Physiology* (pp. 133–280). Berlin: Springer-Verlag.

Lin, T.-Y., Luo, J., Shinomiya, K., Ting, C.-Y., Lu, Z., Meinertzhagen, I. A., & Lee, C.-H. (2016). Mapping chromatic pathways in the Drosophila visual system. *Journal of Comparative Neurology*, *524*(2), 213–227.

Lubbock, S. J. (1888). *On the senses, instincts, and intelligence of animals*. London: Kegan Paul.

Ma, X., Edgecombe, G. D., Hou, X., Goral, T., & Strausfeld, N. J. (2015). Preservational Pathways of Corresponding Brains of a Cambrian Euarthropod. *Current Biology*, *25*(22), 2969–2975.

Ma, X., Hou, X., Edgecombe, G. D., & Strausfeld, N. J. (2012). Complex brain and optic lobes in an early Cambrian arthropod. *Nature*, *490*(7419), 258–261.

Maeda-Martinez, A., Belk, D., Obregon, H., & Dumont, H. J. (1997). Large branchiopod assemblages common to Mexico and the United States. *Hydrobiologia*, (359), 45–62.

Marshall, J., & Arikawa, K. (2014). Unconventional colour vision. *Current Biology*, *24*(24), R1150–R1154.

Martin, J. W. (1992). Branchiopoda. In *Microscopic anatomy of invertebrates* (Vol. 9, pp. 25–224).

Mayer, R. (2004). *Effects of temperatre, salinity and predator chemicals on the life history of three populations of Artemia from the Caribbean*. Duke University.

Melnattur, K. V, Pursley, R., Lin, T.-Y., Ting, C.-Y., Smith, P. D., Pohida, T., & Lee, C.-H. (2014). Multiple redundant medulla projection neurons mediate color vision in Drosophila. *Journal of Neurogenetics*, *28*(3-4), 374–388.

Melzer, R. R., Diersch, R., Nicastro, D., & Smola, U. (1997). Compound Eye Evolution: Highly Conserved Retinula and Cone Cell Patterns Indicate a Common Origin of the Insect and Crustacean Ommatidium. *Naturwissenschaften*, *84*(12), 542–544.

Menzel, R. (1979). Spectral sensitivity and color vision in invertebrates. In A. H (Ed.), *Handbook of Sensory Physiology* (VII., pp. 503–580). Berlin, Heidelberg, New York: Springer.

Menzel, R., & Backhaus, W. (1991). Colour vision in insects. In P. Gouras (Ed.), *Vision and visual dysfunction* (Vol. 6, pp. 262–293). New York, NY.

Menzel, R., & Greggers, U. (1985). Natural phototaxis and its relationship to colour vision in honeybees. *Journal of Comparative Physiology A*, *157*(3), 311–321.

Minckley, W. (1973). *Fishes of Arizona*. Phoenix, Arizona: Sims Printing Company Inc.

Morante, J., & Desplan, C. (2008). The Color-Vision Circuit in the Medulla of Drosophila. *Current Biology*, *18*(8), 553–565.

Morehouse, N. I., & Rutowski, R. L. (2010). In the eyes of the beholders: Female choice and avian predation risk associated with an exaggerated male butterfly color. *The American Naturalist*, *176*(6), 768–84.

Nässel, D., Elofsson, R., & Odselius, R. (1978). Neuronal connectivity patterns in the compound eyes of Artemia salina and Daphnia magna (Crustacea: Branchiopoda). *Cell and Tissue Research*, *190*(3), 435–457.

Nilsson, D.-E. (2009). The evolution of eyes and visually guided behaviour. *Philosophical Transactions of the Royal Society of London. Series B, Biological Sciences*, *364*(1531), 2833–47.

Nilsson, D.-E. (2013). Eye evolution and its functional basis. *Visual Neuroscience*, *30*(1-2), 5–20.

Osorio, D., & Vorobyev, M. (2005). Photoreceptor spectral sensitivities in terrestrial

animals: adaptations for luminance and colour vision. *Proceedings. Biological Sciences / The Royal Society*, *272*(1574), 1745–52.

Partridge, J., & Cummings, M. (1999). Adaptations of visual pigments to the aquatic environment. In S. Archer, D. MB, E. R. Loew, J. Partridge, & S. Vallerga (Eds.), *Adaptive Mechanisms in the Ecology of Vision* (pp. 251–284). Dordrecht: Kluwer Academic Publishers.

Paulk, A. C., Dacks, A. M., & Gronenberg, W. (2009). Color processing in the medulla of the bumblebee (Apidae: Bombus impatiens). *The Journal of Comparative Neurology*, *513*(5), 441–56.

Pichaud, F., Briscoe, A., & Desplan, C. (1999). Evolution of Color Vision. *Current Opinion in Neurobiology*, *9*, 622–627.

Porter, M. L., Blasic, J. R., Bok, M. J., Cameron, E. G., Pringle, T., Cronin, T. W., & Robinson, P. R. (2011). Shedding new light on opsin evolution. *Proceedings. Biological Sciences / The Royal Society*, (October).

Porter, M. L., Cronin, T. W., McClellan, D. a, & Crandall, K. a. (2007). Molecular characterization of crustacean visual pigments and the evolution of pancrustacean opsins. *Molecular Biology and Evolution*, *24*(1), 253–68.

Protas, M. E., Trontelj, P., & Patel, N. H. (2011). Genetic basis of eye and pigment loss in the cave crustacean , Asellus aquaticus. *PNAS*.

Riley, L. G., & Tsukimura, B. (1998). Yolk Protein Synthesis in the Riceland Tadpole Shrimp , Triops longicaudatus , Measured by In Vitro Incorporation of 3 H-Leucine. *Journal of Experimental Zoology*, *281*, 238–247.

Sabbah, S., Gray, S. M., Boss, E. S., Fraser, J. M., Zatha, R., & Hawryshyn, C. W. (2011). The underwater photic environment of Cape Maclear, Lake Malawi: comparison between rock- and sand-bottom habitats and implications for cichlid fish vision. *The Journal of Experimental Biology*, *214*(Pt 3), 487–500.

Sabbah, S., Troje, N. F., Gray, S. M., & Hawryshyn, C. W. (2013). High complexity of aquatic irradiance may have driven the evolution of four-dimensional colour vision in shallow-water fish. *Journal of Experimental Biology*, *216*(9), 1670–1682.

Salcedo, E., Zheng, L., Phistry, M., Bagg, E. E., & Britt, S. G. (2003). Molecular basis for ultraviolet vision in invertebrates. *The Journal of Neuroscience*, *23*(34), 10873–10878.

Seehausen, O., Terai, Y., Magalhaes, I. S., Carleton, K. L., Mrosso, H. D. J., Miyagi, R., … Okada, N. (2008). Speciation through sensory drive in cichlid fish. *Nature*,

455(7213), 620–6.

Sims, S. J., & Macagno, E. R. (1985). Computer reconstruction of all the neurons in the optic ganglion of Daphnia magna. *The Journal of Comparative Neurology*, *233*(1), 12–29.

Sinakevitch, I., Douglass, J. K., Scholtz, G., Loesel, R., & Strausfeld, N. J. (2003). Conserved and convergent organization in the optic lobes of insects and isopods, with reference to other crustacean taxa. *The Journal of Comparative Neurology*, *467*(2), 150–172.

Smith, F. E., & Baylor, E. (1953). Color responses in the Cladocera and their ecological significance. *American Naturalist*, *87*(832), 49–55.

Smith, K. C., & Macagno, E. R. (1990). UV photoreceptors in the compound eye of Daphnia magna (Crustacea, Branchiopoda). A fourth spectral class in single ommatidia. *Journal of Comparative Physiology A: Neuroethology, Sensory, Neural, and Behavioral Physiology*, *166*(5), 597–606.

Snyder, A. W., Menzel, R., & Laughlin, S. (1973). Structure and function of the fused rhabdom. *Journal of Comparative Physiology*, *87*(2), 99–135.

Solomon, S. G., & Lennie, P. (2007). The machinery of colour vision. *Nat Rev Neurosci*, *8*(4), 276–286.

Somanathan, H., Borges, R. M., Warrant, E. J., & Kelber, A. (2008). Nocturnal bees learn landmark colours in starlight. *Current Biology*, *18*(21), R996–R997.

Stavenga, D. G. (2010). On visual pigment templates and the spectral shape of invertebrate rhodopsins and metarhodopsins. *Journal of Comparative Physiology A*, *196*(11), 869–878.

Stavenga, D. G., & Arikawa, K. (2011). Photoreceptor spectral sensitivities of the Small White butterfly Pieris rapae crucivora interpreted with optical modeling. *Journal of Comparative Physiology A*, *197*(4), 373–385.

Stavenga, D. G., Smits, R. P., & Hoenders, B. J. (1993). Simple exponential functions describing the absorbance bands of visual pigment spectra. *Vision Research*, *33*(8), 1011–7.

Stearns, S. C. (1975). Light responses of Daphnia pulex. *Limnology and Oceanography*, *20*, 564–570.

Stevens, M. (2013). *Sensory Ecology, Behavior, and Evolution*. Oxford: Oxford University Press.

Strausfeld, N. J. (2005). The evolution of crustacean and insect optic lobes and the origins of chiasmata. *Arthropod Structure & Development*, *34*(3), 235–256.

Strausfeld, N. J. (2012). *Arthropod brains: evolution, functional elegance, and historical significance*. Belknap Press of Harvard University Press Cambridge, MA.

Theobald, J. C., Greiner, B., Wcislo, W. T., & Warrant, E. J. (2006). Visual summation in night-flying sweat bees: A theoretical study. *Vision Research*, *46*(14), 2298–2309.

Thoen, H. H., How, M. J., Chiou, T.-H., & Marshall, J. (2014). A Different Form of Color Vision in Mantis Shrimp. *Science*, *343*(6169), 411–413.

Thorp, J. H., & Covich, A. P. (2009). *Ecology and classification of North American freshwater invertebrates*. Academic Press.

Toomey, M. B., & McGraw, K. J. (2009). Seasonal, sexual, and quality related variation in retinal carotenoid accumulation in the house finch (Carpodacus mexicanus). *Functional Ecology*, *23*(2), 321–329.

Wakakuwa, M., Stavenga, D. G., & Arikawa, K. (2007). Spectral Organization of Ommatidia in Flower-visiting Insects. *Photochemistry and Photobiology*, *83*(1), 27–34.

Warrant, E. J. (1999). Seeing better at night: life style, eye design and the optimum strategy of spatial and temporal summation. *Vision Research*, *39*(9), 1611–1630.

Warrant, E. J. (2005). Invertebrate vision in dim light. In E. J. Warrant & D.-E. Nilsson (Eds.), *Invertebrate Vision* (pp. 83–121). Cambridge: Cambridge University Press.

Warrant, E. J., Kelber, A., Gislén, A., Greiner, B., Ribi, W., & Wcislo, W. T. (2004). Nocturnal Vision and Landmark Orientation in a Tropical Halictid Bee. *Current Biology*, *14*(15), 1309–1318.

Warrant, E. J., & Nilsson, D.-E. (1998). Absorption of white light in photoreceptors. *Vision Research*, *38*(2), 195–207.

Williams, D. D. (2005). *The Biology of Temporary Waters*. Oxford University Press.

Wyszecki, G., & Stiles, W. S. (1982). *Color science* (Vol. 8). Wiley New York.

Wyszecki, G., & Stiles, W. S. (2000). Color Science: Concepts and Methods, Quantitative Data and Formulae. 2000. Wiley-Interscience, New York.

APPENDIX

A. GREENHOUSE AND MIMIMUM PHOTON FLUX FOR BEHAVIORAL TESTS

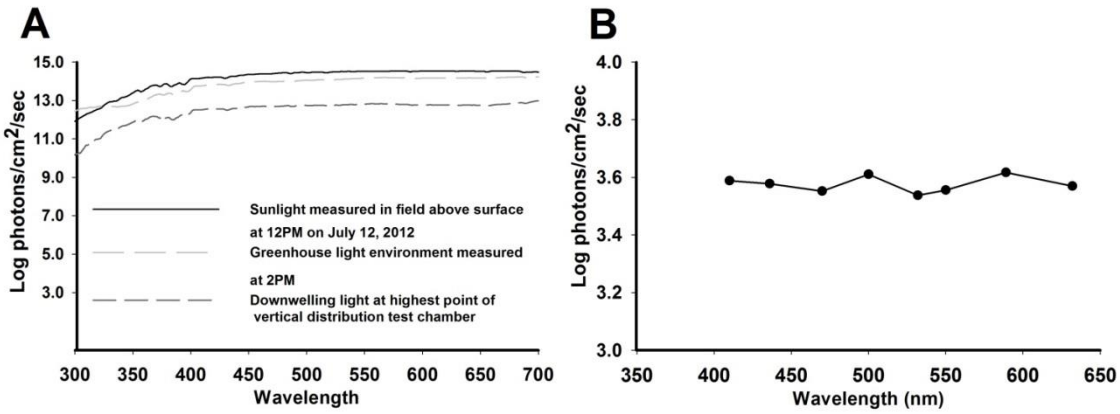

(A) Greenhouse Light Environment. Irradiance in greenhouse used for vertical distribution behavioral tests (B) Minimum photon flux at each wavelength calibrated for behavioral response index tests. This was achieved using non-reflective absorptive neutral density filters to the nearest 0.1 OD unit (Edmund Optics) while minimizing total number of filters in the path length.

B. DIFFUSE ATTENUATION COEFFICIENTS OF DOWNWARD IRRADIANCE

Localized diffuse attenuation coefficients of downward irradiance, shown here for comparison to other bodies of water using the Jerlov Scale. The first row presents median attenuation coefficients at 1.0cm for ephemeral pools in Arizona, measured at 1nm intervals, and binned here to 25 nm intervals for comparison with values reproduced from ref. (Jerlov, 1976), with permission from Elsevier. Note that ref. (Jerlov, 1976) use attenuation in the upper 10 meters of the water column, interpolated here to 1cm. These values are displayed graphically in figure S3. These bodies of water range from the clearest (type I) to coastal and heavily attenuating (type 9).

Water type	Wavelength (nm)															
	310	**350**	**375**	**400**	**425**	**450**	**475**	**500**	**525**	**550**	**575**	**600**	**625**	**650**	**675**	**700**
Median ephemeral pool attenuation **(cm^{-1})**	NA	5.89	2.00	1.21	0.923	0.758	0.631	0.549	0.483	0.430	0.373	0.323	0.293	0.270	0.251	0.242
I **(cm^{-1})**	1.50 $x10^{-4}$	6.20 $x10^{-5}$	3.80 $x10^{-5}$	2.80 $x10^{-5}$	2.20 $x10^{-5}$	1.90 $x10^{-5}$	1.80 $x10^{-5}$	2.70 $x10^{-5}$	4.30 $x10^{-5}$	6.30 $x10^{-5}$	8.90 $x10^{-5}$	2.35 $x10^{-4}$	3.05 $x10^{-4}$	3.60 $x10^{-4}$	4.20 $x10^{-4}$	5.60 $x10^{-4}$
IA **(cm^{-1})**	1.80 $x10^{-4}$	7.80 $x10^{-5}$	5.20 $x10^{-5}$	3.80 $x10^{-5}$	3.10 $x10^{-5}$	2.60 $x10^{-5}$	2.50 $x10^{-5}$	3.20 $x10^{-5}$	4.80 $x10^{-5}$	6.70 $x10^{-5}$	9.40 $x10^{-5}$	2.40 $x10^{-4}$	3.10 $x10^{-4}$	3.70 $x10^{-4}$	4.30 $x10^{-4}$	5.70 $x10^{-4}$
IB **(cm^{-1})**	2.20E $x10^{-4}$	1.00 $x10^{-4}$	6.60 $x10^{-5}$	5.10 $x10^{-5}$	4.20 $x10^{-5}$	3.60 $x10^{-5}$	3.30 $x10^{-5}$	4.20 $x10^{-5}$	5.40 $x10^{-5}$	7.20 $x10^{-5}$	9.90 $x10^{-5}$	2.45 $x10^{-4}$	3.15 $x10^{-4}$	3.75 $x10^{-4}$	4.35 $x10^{-4}$	5.80 $x10^{-4}$
II **(cm^{-1})**	3.70 $x10^{-4}$	1.75 $x10^{-4}$	1.22 $x10^{-4}$	9.60 $x10^{-5}$	8.10 $x10^{-5}$	6.80 $x10^{-5}$	6.25 $x10^{-5}$	7.00 $x10^{-5}$	7.60 $x10^{-5}$	8.90 $x10^{-5}$	1.15 $x10^{-4}$	2.60 $x10^{-4}$	3.35 $x10^{-4}$	4.00 $x10^{-4}$	4.65 $x10^{-4}$	6.10 $x10^{-4}$
1 **(cm^{-1})**	1.80 $x10^{-3}$	1.20 $x10^{-3}$	8.00 $x10^{-4}$	5.10 $x10^{-4}$	3.60 $x10^{-4}$	2.50 $x10^{-4}$	1.70 $x10^{-4}$	1.40 $x10^{-4}$	1.30 $x10^{-4}$	1.20 $x10^{-4}$	1.50 $x10^{-4}$	3.00 $x10^{-4}$	3.70 $x10^{-4}$	4.50 $x10^{-4}$	5.10 $x10^{-4}$	6.50 $x10^{-4}$
3 **(cm^{-1})**	2.40 $x10^{-3}$	1.70 $x10^{-3}$	1.10 $x10^{-3}$	7.80 $x10^{-4}$	5.40 $x10^{-4}$	3.90 $x10^{-4}$	2.90 $x10^{-4}$	2.20 $x10^{-4}$	2.00 $x10^{-4}$	1.90 $x10^{-4}$	2.10 $x10^{-4}$	3.30 $x10^{-4}$	4.00 $x10^{-4}$	4.60 $x10^{-4}$	5.60 $x10^{-4}$	7.20 $x10^{-4}$
5 **(cm^{-1})**	3.50 $x10^{-3}$	2.30 $x10^{-3}$	1.60 $x10^{-3}$	1.10 $x10^{-3}$	7.80 $x10^{-4}$	5.60 $x10^{-4}$	4.30 $x10^{-4}$	3.60 $x10^{-4}$	3.10 $x10^{-4}$	3.00 $x10^{-4}$	3.30 $x10^{-4}$	4.00 $x10^{-4}$	4.80 $x10^{-4}$	5.40 $x10^{-4}$	6.50 $x10^{-4}$	8.00 $x10^{-4}$
7 **(cm^{-1})**	NA	3.00 $x10^{-3}$	2.10 $x10^{-3}$	1.60 $x10^{-3}$	1.20 $x10^{-3}$	8.90 $x10^{-4}$	7.10 $x10^{-4}$	5.80 $x10^{-4}$	4.90 $x10^{-4}$	4.60 $x10^{-4}$	4.60 $x10^{-4}$	4.80 $x10^{-4}$	5.40 $x10^{-4}$	6.30 $x10^{-4}$	7.80 $x10^{-4}$	9.20 $x10^{-4}$
9 **(cm^{-1})**	NA	3.90 $x10^{-3}$	3.00 $x10^{-3}$	2.40 $x10^{-3}$	1.90 $x10^{-3}$	1.60 $x10^{-3}$	1.23 $x10^{-3}$	9.90 $x10^{-4}$	7.80 $x10^{-4}$	6.30 $x10^{-4}$	5.80 $x10^{-4}$	6.00 $x10^{-4}$	6.50 $x10^{-4}$	7.60 $x10^{-4}$	9.20 $x10^{-4}$	1.10 $x10^{-3}$

C. MINIMUM INTENSITY MODELING

Here we develop equations **[2a]** and **[2b]** presented in our main text. The fundamental equation is the same, and is presented as eq. [2] in (Nilsson, 2013), using radians and as eq. [A1] in (Warrant, 1999) using degrees. We use the original equation numbering scheme from those sources, but change subscripts to avoid confusion between compound (subscript *c*), and median (subscript *m)* eyes.

$$N_{min} = \Omega \cdot Z \cdot a \cdot \Delta t \cdot I_{min}, \quad \textbf{eq.[2] from} \text{ (Nilsson, 2013)}$$

$$N_{min} = \Omega_T \cdot \frac{\pi}{4} D^2 n_f \cdot \gamma \cdot \Delta t \cdot I_{min}, \quad \textbf{eq.[A1]from}\text{(Warrant, 1999)}$$

N_{min} is the photon sample captured during one integration time. Ω is the solid angle sampled by the light-sensitive structure, Z is the area over which photons are captured and is equivalent to $\frac{\pi}{4} D^2$, where D is the diameter of the light detecting structure. a is the fraction of received photons which are detected, Δt is the integration time, and I_{min} is intensity (photon flux). Because photon shot noise follows Poisson statistics, $N_{min} \geq \frac{N}{\sqrt{N}}$ to generate a signal to noise ratio greater than photon shot noise. $\frac{N}{\sqrt{N}} = \sqrt{N}$. Therefore, in order to elicit behavior, I_{min}, must large enough so that $N_{min} \geq \sqrt{N}$. Since our behavioral assays describe the probability of a behavioral outcome at each intensity, we model N_{min} to determine whether a given intensity can generate a detectable signal: noise ratio. As (Nilsson, 2013) explores hypothetical behavior, assumptions for N_{min} were modeled using a confidence factor with a fixed probability.

In equation**[A1],** (Warrant, 1999) uses the term γ, which is equivalent to a in equation **[2]** from (Nilsson, 2013). Note that for apposition compound eyes, the number of lenses, $n_f = 1$. In superposition eyes, such as those of the nocturnal hawkmoth, *Deilephila*

elpenor, n_f is composed of multiple lenses that contribute to a single effective aperture (Table 1).

For both median and compound eyes, we solve for I_{min}.

For **median eyes, equation [2a from our main text],** we substitute: $\Omega = 2\pi\left(1 - cos\frac{\Delta\rho_m}{2}\right)$, where $\Delta\rho_m$ is the apex angle in radians of the modeled three dimensional cone of light for the median eye. $Z = \frac{\pi}{4}D^2$, where D is the diameter of the median eye. $a = \kappa\tau\left(\frac{kl}{2.3+kl}\right)$, where κ is the quantum efficiency of transduction, τ is the transmission through eye media, k is the photoreceptor absorption coefficient. The term $\left(\frac{kl}{2.3+kl}\right)$ incorporates a correction established by (Warrant & Nilsson, 1998) for k values, which are found at *peak* absorbance of a visual pigment, which would lead to unrealistic estimates of sensitivity for all wavelengths which are not at peak sensitivity.

From these steps we obtain the equation presented in the main text for median eyes:

$$I_{min} = \frac{N_{min}}{2\pi\left(1-\cos\frac{\Delta\rho_m}{2}\right)\pi\left(\frac{D_m}{2}\right)^2\kappa\tau\left(\frac{kl}{2.3+kl}\right)\Delta t} \qquad \textbf{[2a from main text]}$$

In order to further develop [A1] for compound apposition eyes, and to incorporate summation from multiple ommatidia (Warrant, 1999) use the following considerations. First, note that Ω_T in **eq. [A1]** represents a solid angle represented by multiple photoreceptors,

$$\Omega_T = n_r n_c \Omega, \quad \textbf{eq.[A3] from} \text{ (Warrant, 1999)}$$

Where n_r is the number of photoreceptors contributing to a laminar cartridge, and n_c is the number of summed laminar cartridges, and Ω is the solid angle sampled by each photoreceptor.

To approximate Ω of each photoreceptor (Warrant, 1999) use the following:

$$\Omega = 1.13\left(\frac{d}{f}\right)^2, \qquad \textbf{eq.[A4] from} \text{ (Warrant, 1999)}$$

where d is the diameter of a photoreceptor, and f is the focal length. As will be seen, the solid angle estimate is further refined in subsequent steps. Meanwhile equations[A3-A6] from (Warrant, 1999) are further developed to employ a realistic volume summation function, so that:

$$n_c = 1.426\left(\frac{\Delta\rho_{Sum}}{\Delta\phi}\right)^2, \qquad \textbf{eq.[A8] from} \text{ (Warrant, 1999)}$$

Where $\Delta\rho_{sum}$is the input spatial summation function from multiple photoreceptors. n_c is the number of summed input cartridges.

Substituting eq. [A3], [A4], [A8], and γ, (Warrant, 1999) then obtain:

$N_{min} = 1.269 \cdot \left(\frac{d \cdot D \cdot \Delta\rho_{Sum}}{\Delta\phi \cdot f}\right)^2 \cdot \gamma \cdot \Delta t \cdot I_{min}$ **eq.**[**6b] from** (Warrant, 1999)

Equation [**6b]** was later updated by (Theobald et al., 2006) to incorporate summation of first order monopolar neurons at the output level of the lamina, from laminar circuits. We use eqs. [2a] from (Theobald et al., 2006):

$N_{min} = 1.269\left(\frac{\Delta\rho_{sum}}{\Delta\phi}\right)^2 \Delta\rho_c^2 {D_c}^2 \kappa\tau\left(\frac{kl}{2.3+kl}\right)\Delta t\, I_{min}$, **eq.**[**2] from** (Theobald et al., 2006)

For **compound eyes**, **equation [2b from our main text],** rearranging eq. [2] for I_{min},

$I_{min} = \frac{N_{min}}{1.269\left(\frac{\Delta\rho_{sum}}{\Delta\phi}\right)^2 \Delta\rho_c^2 {D_c}^2 \kappa\tau\left(\frac{kl}{2.3+kl}\right)\Delta t}$, **[2b from main text]**

We then use $n_c = \frac{\pi\Delta\rho_{sum}^2}{4\delta}$, **eq.**[**5] from** (Theobald et al., 2006)

Where δ approximates the solid angular area in space viewed by a single optic cartridge in square degrees. The most accurate approximation of this solid angle would be to use $\delta = 2\pi\left(1 - cos\frac{\Delta\phi}{2}\right)$. Further, we know monopolar neurons in branchiopods connect to multiple laminar cartridges (Figure. X A, B), and have modified this term so it instead approximates the solid angle viewed by ΔϕC, where Δϕ is the interommatidial angle, and C is the packing ratio, found by (Strausfeld, 2005), to be 3:1 in Notostracans, and 6.3:1 in Anostracans. Rearranging to solve for $\Delta\rho_{sum}$, and incorporating this packing ratio, we develop this equation for what is known about the branchiopod visual system. We have estimated n_c (Table 1) and use it to model $\Delta\rho_{Sum}$:

$$\boldsymbol{\Delta}\rho_{sum} = \sqrt{\frac{4n_c\delta\mathrm{C}}{\pi}} \qquad \textbf{[2c from main text]}$$

D. ALL ABSORPTANCE MODEL COMPARISONS CONSIDERED FOR *S. MACKINI* AND *T. LONGICAUDATUS*

This appendix corresponds to Table 2. Tiered photoreceptor arrays were modeled for each species and sex using parameters from Equations 3a and 3b. A_i/A, relative area of photoreceptor in cross-section. SSH, rhodopsin visual pigment template (Stavenga et al., 1993). GFRKD, rhodopsin visual pigment template (Govardovskii et al., 2000). All models considered are displayed here for each species and sex, and only the best models (>0.02 $wAIC_c$) were included in the main text. Evidence ratios were calculated relative to the best model for each species and sex. Models with ambiguous $wAIC_c$ (evidence ratio < 2.0) are indicated by (^{a}). Models with low support relative to the best model (evidence ratio > 2.0) are indicated by (^{b}).

Species/Sex	Model	λ max 1	λ max 2	λ max 3	λ max 4	λ max 5	A1/A	A2/A	A3/A	A4/A	A5/A	AICc	ΔAICc	wAICc	Evidence Ratio
T. longicaudatus	4, SSH	362	415	499	606	-	0.16	0.34	0.26	0.25	-	-30.4	0	0.47	-
	4, GFKRD[a]	365	414	498	606	-	0.16	0.35	0.25	0.24	-	-30.2	0.18	0.429	1.097
	3, SSH[b]	392	489	602	-	-	0.27	0.49	0.23	-	-	-26.9	3.51	0.081	5.78
	3, GFKRD[b]	393	488	602	-	-	0.28	0.5	0.23	-	-	-24	6.39	0.019	24.374
	5, GFKRD[b]	364	412	496	598	630	0.15	0.35	0.26	0.19	0.05	-4.8	25.59	<0.01	360830
	5, SSH[b]	361	412	498	599	630	0.14	0.34	0.26	0.21	0.05	-4.6	25.84	<0.01	409014
	2, SSH[b]	437	579	-	-	-	0.56	0.44	-	-	-	10.7	41.14	<0.01	8.6E+08
	2, GFKRD[b]	437	578	-	-	-	0.57	0.43	-	-	-	12.4	42.81	<0.01	2E+09
	1, SSH[b]	540	-	-	-	-	1	-	-	-	-	28.6	59.01	<0.01	6.5E+12
	1, GFKRD[b]	540	-	-	-	-	1	-	-	-	-	30.2	60.56	<0.01	1.4E+13
S. mackini ♂	4, SSH	355	430	528	586	-	0.31	0.16	0.21	0.32	-	-43.7	0	0.881	-
	4, GFKRD[b]	357	429	531	585	-	0.3	0.18	0.23	0.29	-	-39.7	4	0.119	7.402
	3, SSH[b]	362	447	559	-	-	0.28	0.15	0.56	-	-	-26.8	16.9	<0.01	4666.39
	3, GFKRD[b]	364	444	559	-	-	0.28	0.17	0.55	-	-	-26	17.75	<0.01	7164.18
	5, GFKRD[b]	345	381	437	529	586	0.22	0.09	0.16	0.2	0.32	-22.4	21.33	<0.01	42741
	5, SSH[b]	342	383	437	531	587	0.24	0.08	0.15	0.21	0.32	-2.1	41.61	<0.01	1.1E+09
	2, SSSH[b]	417	556	-	-	-	0.65	0.35	-	-	-	1.7	45.43	<0.01	7.3E+09
	2, GFKRD[b]	419	555	-	-	-	0.66	0.34	-	-	-	3.5	47.22	<0.01	1.8E+10
	1, SSH[b]	540	-	-	-	-	1	-	-	-	-	27.9	71.62	<0.01	3.6E+15
	1, GFKRD[b]	540	-	-	-	-	1	-	-	-	-	30	73.68	<0.01	1E+16
S. mackini ♀	4, SSH	358	426	541	601	-	0.08	0.14	0.53	0.26	-	-52	0	0.548	1
	4, GFKRD[a]	362	428	540	600	-	0.08	0.16	0.51	0.25	-	-51.6	0.39	0.451	1.216
	3, SSH[b]	396	538	597	-	-	0.13	0.58	0.29	-	-	-	13.2	<0.01	736.748

3, GFKRD[b]	403	536	595	-	-	0.14	0.56	0.3	-	-	-38.8 -34.3	17.74	<0.01	7098.36
5, GFKRD[b]	330	370	431	536	597	0.04	0.1	0.15	0.43	0.28	-29.6	22.4	<0.01	73234.1
5, SSH[b]	352	410	453	541	601	0.07	0.1	0.07	0.5	0.26	-27.6	24.43	<0.01	201637
2, SSSH[b]	418	560	-	-	-	0.18	0.82	-	-	-	-19.3	32.71	<0.01	1.3E+07
2, GFKRD[b]	423	560	-	-	-	0.19	0.81	-	-	-	-18.3	33.65	<0.01	2E+07
1, SSH[b]	557	-	-	-	-	1	-	-	-	-	-6.2	45.77	<0.01	8.7E+09
1, GFKRD[b]	555	-	-	-	-	1	-	-	-	-	-2.2	49.79	<0.01	6.5E+10

E. ALL ABSORPTANCE MODEL COMPARISONS CONSIDERED FOR *P. HITOYENSIS* AND *H. SAPIENS*

This appendix corresponds to Table 3. Photoreceptor arrays were modeled for each species and condition using parameters from Equations 4 and 5. A_i/A, relative area of photoreceptor in cross-section, or relative frequency. SSH, rhodopsin visual pigment template (Stavenga et al., 1993). GFRKD, rhodopsin visual pigment template (Govardovskii et al., 2000). All models considered are displayed here for each species and condition, and only the best models (>0.02 $wAIC_c$) were included in the main text. Evidence ratios were calculated relative to the best model for each species and sex. Models with ambiguous $wAIC_c$ (evidence ratio < 2.0) are indicated by ([a]). Models with low support relative to the best model (evidence ratio > 2.0) are indicated by ([b]).

Species/Sex	(Reference) Model	$\lambda_{max\ 1}$	$\lambda_{max\ 2}$	$\lambda_{max\ 3}$	$\lambda_{max\ 4}$	$\lambda_{max\ 5}$	A_1/A	A_2/A	A_3/A	A_4/A	A_5/A	AIC_c	ΔAIC_c	$wAIC_c$	Evidence Ratio
P.hitoyensis	(Beckmann et al., 2015)	484	-	-	-	-	-	-	-	-	-	-	-	0.508	-
	1, GFKRD[a]	481	-	-	-	-	1.0	-	-	-	-	-55.6	0	0.33	-
	1, SSH[a]	481	-	-	-	-	1.0	-	-	-	-	-54.9	0.86	0.143	1.54
	2, GFKRD[b]	481	481	-	-	-	0.70	0.30	-	-	-	-53.2	2.54	0.0159	3.56
	2, SSH[b]	481	481	-	-	-	0.18	0.82	-	-	-	-48.8	6.92	<0.01	31.9
	3, GFKRD[b]	480	480	630	-	-	0.54	0.42	0.03	-	-	-44.9	10.9	<0.01	231.3
	3, SSH[b]	481	481	630	-	-	0.44	0.52	0.04	-	-	-39.6	16.2	<0.01	$3.28x10^3$
	4, GFKRD[b]	330	480	480	630	-	0.04	0.53	0.40	0.03	-	-31.1	24.6	<0.01	$2.23x10^5$
	4, SSH[b]	481	481	481	630	-	0.04	0.60	0.32	0.04	-	-24.3	31.5	<0.01	$6.89x10^6$
	5, GFKRD[b]	330	481	480	480	630	0.04	0.66	0.14	0.13	0.03	-5.63	50.1	<0.01	$7.68x10^{10}$
	5, SSH[b]	481	481	481	481	630	0.10	0.04	0.78	0.04	0.04	1.23	57.0	<0.01	$2.37x10^{12}$
Normal Human (scotopic)	(Wyszecki & Stiles, 2000)	420	497	-	-	-	-	-	-	-	-	-	-	-	-
	2, SSH[a]	421	495	-	-	-	0.16	0.86	-	-	-	-91.3	0	0.500	-
	2, GFKRD[a]	419	495	-	-	-	0.17	0.83	-	-	-	-91.1	0.176	0.458	7.402
	3, SSH[b]	407	493	493	-	-	0.11	0.44	0.44	-	-	-	6.24	0.022	1.09

													85.1		1	
		3, GFKRD[b]	404	493	493	-	-	0.14	0.43	0.43	-	-	-	6.50	0.019	22.59
													84.8		4	
		4, SSH[b]	387	491	491	491	-	0.11	0.26	0.31	0.33	-	-	19.8	<0.01	25.75
													71.5			
		4, GFKRD[b]	392	491	491	491	-	0.13	0.33	0.21	0.33	-	-	20.1	<0.01	2.00 x10^4
													71.2			
		1, SSH[b]	493	-	-	-	-	1	-	-	-	-	-	21.3	<0.01	2.31 x10^4
													70.0			
		1, GFKRD[b]	493	-	-	-	-	1	-	-	-	-	-	23.4	<0.01	4.19 x10^4
													67.9			
		5, SSH[b]	387	491	491	491	491	0.11	0.26	0.28	0.33	0.03	-	45.3	<0.01	1.22 x10^5
													46.1			
		5, GFKRD[b]	392	491	491	491	491	0.13	0.25	0.27	0.33	0.02	-	45.6	<0.01	6.88 x10^9
													45.7			
	Enchanced S-cone Human (scotopic)	(Wyszecki & Stiles, 2000)	420	497	-	-	-	-	-	-	-	-	-	-	-	-
		2, SSH[a]	429	506	-	-	-	0.76	0.24	-	-	-	-	0	0.587	-
													65.6			
		2, GFKRD[a]	429	504	-	-	-	0.75	0.25	-	-	-	-	1.62	0.261	2.25
													64.0			
		3, GFKRD[b]	375	433	507	-	-	0.27	0.54	0.20	-	-	-	3.79	0.088	6.65
													61.8			
		3, SSH[b]	383	436	509	-	-	0.28	0.53	0.20	-	-	-	4.48	0.062	9.38
													61.1		6	
		4, GFKRD[b]	388	432	497	544	-	0.22	0.55	0.20	0.03	-	-	14.6	<0.01	1.49 x10^3
													51.0			
		4, SSH[b]	368	430.	498	541	-	0.29	0.52	0.16	0.03	-	-	16.4	<0.01	3.72 x10^3
													49.1			
		1, SSH[b]	427	427	427	499	567	0.26	0.26	0.26	0.20	0.01	-	37.0	<0.01	1.06 x10^8
													28.6			
		1, GFKRD[b]	367	429	429	450	558	0.27	0.28	0.28	0.16	0.01	-	40.2	<0.01	5.35 x10^8
													25.4			
		5, SSH[b]	453	-	-	-	-	1.0	-	-	-	-	5.05	70.6	<0.01	2.16 x10^{15}
		5, GFKRD[b]	454	-	-	-	-	1.0	-	-	-	-	5.74	71.3	<0.01	3.06

$x10^{15}$

F. ALL ABSORPTANCE MODEL COMPARISONS CONSIDERED FOR *D. MAGNA* AND *P. XUTHUS*

This appendix corresponds to Table 4. Photoreceptor arrays were modeled for each species and condition using parameters from Equations 4 and 5. A_i/A, relative area of photoreceptor in cross-section, or relative frequency. SSH, rhodopsin visual pigment template (Stavenga et al., 1993). GFRKD, rhodopsin visual pigment template (Govardovskii et al., 2000). All models considered are displayed here for each species and condition, and only the best models (>0.02 $wAIC_c$) were included in the main text. Evidence ratios were calculated relative to the best model for each species and sex. Models with ambiguous $wAIC_c$ (evidence ratio < 2.0) are indicated by ([a]). Models with low support relative to the best model (evidence ratio > 2.0) are indicated by ([b]).

Species/Sex	(Reference) Model	$\lambda_{max\ 1}$	$\lambda_{max\ 2}$	$\lambda_{max\ 3}$	$\lambda_{max\ 4}$	$\lambda_{max\ 5}$	A_1/A	A_2/A	A_3/A	A_4/A	A_5/A	AIC_c	ΔAIC_c	$wAIC_c$	Evidence Ratio
D. magna (Tiered absorptance)	(K. C. Smith & Macagno, 1990)	356	440	521	592	-	-	-	-	-	-	-	-	-	-
	4, SSH[a]	362	442	518	587	-	0.52	0.21	0.12	0.15	-	-46.2	0	0.98	-
	3, SSH[b]	367	455	560	-	-	0.50	0.22	0.28	-	-	-38.3	7.96	0.02	53.6
	4, GFKRD[b]	364	437	509	582	-	0.50	0.21	0.12	0.16	-	-33.3	13.0	<0.01	656.0
	3, GFKRD[b]	370	453	558	-	-	0.49	0.23	0.28	-	-	-31.8	14.4	<0.01	$1.35\ x10^3$
	5, GFKRD[b]	353	381	446	523	591	0.35	0.16	0.23	0.13	0.14	-27.7	18.5	<0.01	$1.05\ x10^4$
	5, SSH[b]	358	395	450	528	594	0.48	0.07	0.21	0.12	0.12	-26.0	20.2	<0.01	$2.48\ x10^4$
	2, SSH[b]	378	492	-	-	-	0.70	0.30	-	-	-	4.08	50.3	<0.01	$8.45\ x10^{10}$
	2, GFKRD[b]	380	488	-	-	-	0.69	0.31	-	-	-	5.71	52.0	<0.01	$1.91\ x10^{11}$
	1, SSH[b]	440	-	-	-	-	1.0	-	-	-	-	30.0	76.2	<0.01	$3.52\ x10^{16}$
	1, GFKRD[b]	440	-	-	-	-	1.0	-	-	-	-	31.1	77.3	<0.01	$6.11\ x10^{16}$
P. xuthus (Tiered absorptance)	(Arikawa et al., 1987)	360	390/ 400	460	520	600	-	-	-	-	-	-	-	-	-
	2, SSH[a]	429	529	-	-	-	0.48	0.52	-	-	-	-34.9	0	0.726	-
	3, SSH[b]	429	505	559	-	-	0.56	0.23	0.21	-	-	-31.4	3.48	0.128	5.69
	2, GFKRD[b]	422	529	-	-	-	0.49	0.51	-	-	-	-30.5	4.39	0.0808	8.98
	3, GFKRD[b]	418	491	548	-	-	0.50	0.23	0.28	-	-	-30.0	4.81	0.0655	11.08
	4, SSH[b]	429	498	542	604	-	0.60	0.21	0.15	0.04	-	-19.3	15.6	<0.01	$2.42\ x10^3$
	4, GFKRD[b]	418	4823	532	591	-	0.55	0.22	0.18	0.06	-	-18.3	16.6	<0.01	$4.03\ x10^3$
	5, GFKRD[b]	425	490	536	536	600	0.57	0.21	0.12	0.06	0.05	-2.00	32.8	<0.01	$1.35\ x10^7$
	5, SSH[b]	436	506	547	547	616	0.63	0.21	0.10	0.03	0.03	-0.27	34.6	<0.01	$3.24\ x10^7$

	1, SSH[b]	479	-	-	-	-	1.0	-	-	-	-	5.05	39.9	<0.01	4.63 x10[8]
	1, GFKRD[b]	471	-	-	-	-	1.0	-	-	-	-	13.4	48.2	<0.01	2.94 x10[10]
P. xuthus (Absorbance)	(Arikawa et al., 1987)	360	390/ 400	460	520	600	-	-	-	-	-	-	-	-	-
	5, GFKRD[a]	346	381	457	529	586	0.10	0.25	0.32	0.20	0.12	-50.4	0	0.653	-
	3, SSH[b]	371	462	557	-	-	0.35	0.37	0.28	-	-	-47.8	2.62	0.176	3.71
	4, GFKRD[b]	348	385	465	559	-	0.12	0.26	0.36	0.25	-	-46.6	3.83	0.0963	6.77
	4, SSH[b]	353	387	467	560	-	0.16	0.22	0.37	0.26	-	-45.7	4.72	0.0617	10.6
	5, SSH[b]	349	380	461	538	595	0.11	0.24	0.34	0.22	0.10	-42.0	8.41	<0.01	67.2
	3, GFKRD[b]	373	459	555	-	-	0.35	0.37	0.28	-	-	-40.1	10.4	<0.01	174.0
	2, SSH[b]	392	512	-	-	-	0.48	0.52	-	-	-	3.00	53.4	<0.01	3.93 x10[11]
	2, GFKRD[b]	393	509	-	-	-	0.49	0.51	-	-	-	5.04	55.4	<0.01	1.09x10[11]
	1, SSH[b]	480	-	-	-	-	1.0	-	-	-	-	33.0	83.4	<0.01	1.30 x10[18]
	1, GFKRD[b]	480	-	-	-	-	1.0	-	-	-	-	34.4	84.7	<0.01	2.52 x10[18]